Article

Dynamics of the Land–Sea Breeze System and the Surface Current Response in South-West Australia

Syeda Rafiq, Charitha Pattiaratchi *[ID] and Ivica Janeković[ID]

Oceans Graduate School & the UWA Oceans Institute, The University of Western Australia, Perth 6009, Australia; syeda.rafiq@research.uwa.edu.au (S.R.); ivica.janekovic@uwa.edu.au (I.J.)
* Correspondence: chari.pattiaratchi@uwa.edu.au; Tel.: +61-8-6488-3179

check for updates

Abstract: The land–sea breeze (LSB) system, driven by the thermal contrast between the land and the adjacent ocean is a widely known atmospheric phenomenon, which occurs in coastal regions globally. South-west Australia experiences a persistent and one of the strongest LSB systems globally with maximum wind speeds associated with the LSB system often exceeding 15 ms^{-1}. In this paper, using field measurements and numerical simulations, we examine: (1) the local winds associated with the land–sea breeze with an emphasis on the ocean; and, (2) the response of the surface currents to the diurnal wind forcing. The measurements indicated that the wind speeds decreased between midnight and 0400 and increased rapidly after 1100, reaching maxima >10 ms^{-1} around 1800) associated with the sea breeze and decreased to midnight. Wind directions were such that they were blowing from south-east (120°) in the morning and changed to almost southerly (~200°) in the afternoon. Decomposition of the wind record to the diurnal and synoptic components indicated that the diurnal component of winds (i.e., LSB) was oriented along the south-west to north-east axis. However, the stronger synoptic winds were from the south-east to south quadrant and in combination with the LSB, the winds consisted of a strong southerly component. We examined the evolution, horizontal extent, and propagation properties of sea breeze fronts for characteristic LSB cycles and the sea breeze cell propagating offshore and inland. The results indicated that the sea breeze cell was initiated in the morning in a small area, close to 33° S, 115.5° E, with a width of ~25 km and expanded onshore, offshore and alongshore. The sea breeze cell expanded faster (30 kmh^{-1}) and farther (120 km) in the offshore direction than in the onshore direction (10 kmh^{-1} and 30–40 km). Winds during the LSB cycle followed a counterclockwise rotation that was also reflected in the surface currents. The winds and surface currents rotated anticlockwise with the surface currents responding almost instantaneously to changes in wind forcing but were modified by topography. The diurnal surface currents were enhanced due to the resonance between the LSB forcing and the inertial response.

Keywords: land–sea breeze system; offshore extent; south-west Australia; surface currents; numerical simulation

1. Introduction

The land–sea breeze (LSB) is a phenomenon that occurs along approximately two-thirds of the global coastline [1]. They have been described from the period of Greek philosophers [2] to early explorers such as William Dampier [3] to scientific accounts by Davis et al. [4] and extending to the present [5,6]. The descriptions by Dampier are somewhat relevant to this paper as he most likely experienced the strong sea breezes whilst exploring Western Australia and, in particular, Shark Bay (which was named by Dampier) and northern Western Australia that experience strong sea breezes [7]. Dampier [8] as quoted in Simpson [5] described the sea breeze as:

"These sea breezes do commonly rise in the Morning about Nine-a-Clock, sometimes sooner, sometimes later: they first approach the Shore so gently, as they were afraid to come near it, and oft-times they make some faint Breathings, and as if not willing to offend, they make a halt, and seem ready to retire. I have waited many a time both Ashore to receive the Pleasure, and at Sea to take the Benefit of it.

It comes in a fine, small, black Curl upon the Water, when, as all the Sea between it and the Shore not yet reached by it, is as smooth and even as Glass in comparison; in half an Hours's time after it has reached the Shore it fans pretty briskly, and so increaseth gradually till Twelve a-Clock, then it is commonly strongest, and lasts so till Two or Three a very brisk Gale; about Twelve at Noon it also veers off to Sea Two or Three points, or more in very fine Weather . . . ".

This description from Dampier accurately describes the land–sea breeze (LSB) system including veering of the winds with time [5]. It can affect the local waves, coastal circulation and mixing, sediment transport, and beach morphology [7,9–12]. The sea breeze can trigger thunderstorms, provide relief from oppressive hot weather, provide moisture for fog, and improve or reduce air quality near the coast. For example, the local sea breeze in south-west Australia is named the 'Fremantle doctor', as it provides relief from the hot weather in summer ('Ashore to receive the Pleasure': as described by Dampier above).

Although the LSB provides a diurnal modulation in wind speed and direction, and ocean currents respond to this variation in forcing, the relationship between the surface wind stress and the current response is nonlinear and the land boundary also influences the current response. Studies have shown that only ~50% of the diurnal current variance is related to the diurnal wind stress through linear correlation [12]. Other processes, including the action of eddies and upwelling and downwelling response to the alongshore wind stress also drive the coastal circulation [13]. Diurnal forcing also causes diurnal variability in the upwelling and downwelling processes [14]. These physical processes are important for transport of buoyant material [15], nutrient distribution [16], pollution transfer [17], and water exchange [18] in the coastal zone. The redistribution of nutrients affects primary production, which is important for maintaining marine biodiversity and fisheries. A study of the LSB and its effect on coastal currents would enhance the knowledge required for better management and sustainable development of the coastal ecosystem.

The temperature difference between the land and the ocean drives the LSB system [6,9,19]. The incoming solar radiation during the day causes differential heating of the land because the specific heat capacity of the land is lower than that of the adjacent ocean. This differential heating causes warm air to rise over the land, which creates a low-pressure region (Figure 1a). In general, the ocean temperature is lower than the land temperature; thus, a high-pressure zone exists over the ocean. This pressure gradient between the land and the ocean results in the sea breeze, which transports cooler air from the ocean onshore (Figure 1a). During the night, the land loses heat, so it is cooler than the ocean; the pressure gradient is reversed, and the land breeze transports air from the land to the ocean. Hence, it is the pressure gradient between the land and the ocean that controls the formation, direction, and intensity of the sea breeze [5].

Theoretical and observational studies of sea breeze circulations have been undertaken many regions globally: south-eastern Australia [9]; Indonesia [20]; Brunei Darussalam [21]; Japan [22]; California [23,24]; Florida's Atlantic and Gulf coasts [25,26]; New Jersey coast [14]; Chile [27]; Columbia [28]; Sardinia [29]; southern Spain [30], southern France [31]; Adriatic Sea [32]; the Persian Gulf [33]; the Red Sea [34]; and, the southern North Sea [35]. Gille et al. [36] examined global winds measured using scatterometers and indicated that sea breezes are prevalent in tropical and sub-tropical coastlines globally. Based on these studies, the LSB circulation can be summarised as follows: (1) a pressure gradient force, which is directed from sea to land, pushes a shallow layer of marine air inland (Figure 1a); (2) a convective sea breeze cell is initiated close to the coast and expands both onshore and offshore (Figure 1b). The cell closest to the shore has shoreward flow at the surface, rising air currents inland, and sinking air offshore. An area of divergence is present on the ocean surface (Figure 1b) and

expands offshore [37]; (3) the sea breeze front typically [34] occurs on land dependent on synoptic flow. When the terrestrial and ocean air converge it is often associated with sharp changes in the moisture, temperature, and wind speed and direction. The front behaves like a density current [5]; and (4) the synoptic-scale circulation can affect the LSB circulation.
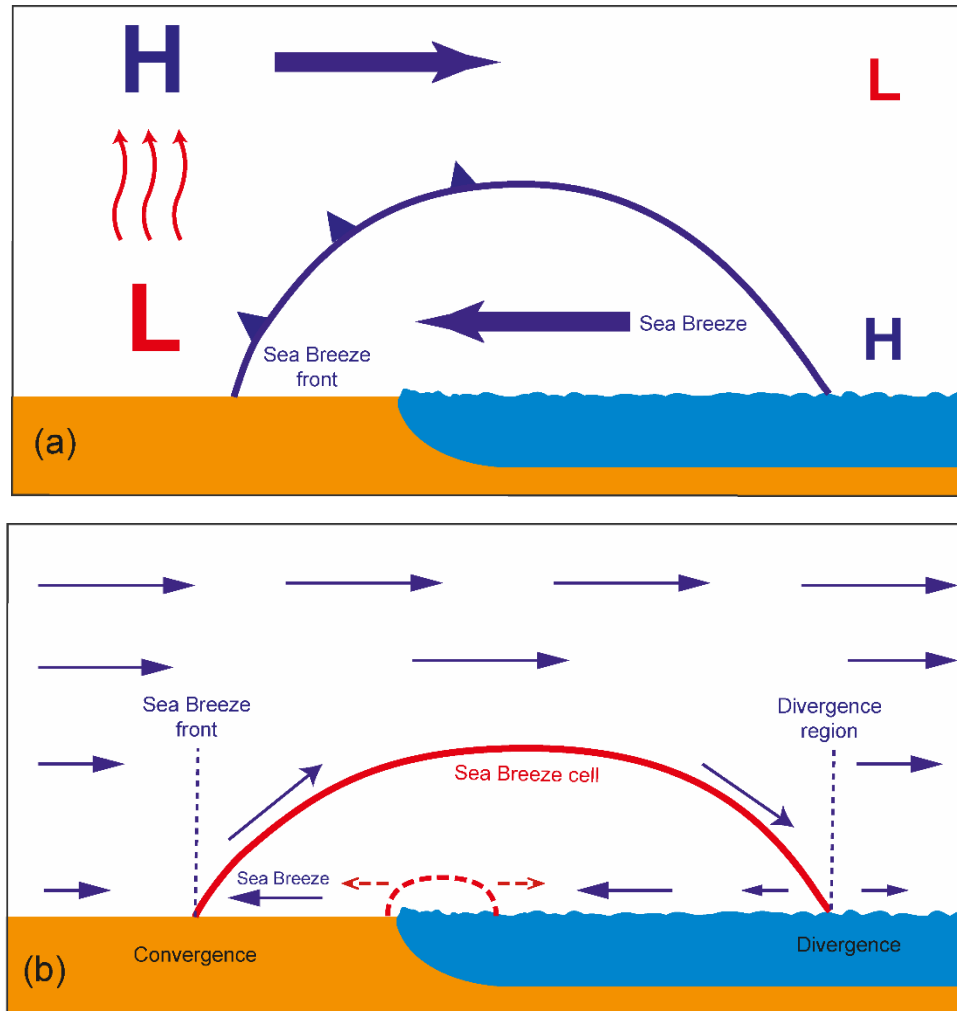
Figure 1. (**a**) Schematic of the sea breeze circulation perpendicular to the coast showing the sea breeze front propagating on land and the distribution of pressure. Here, the synoptic winds blow in an offshore direction; (**b**) schematic of the sea breeze cell showing areas of convergence and divergence. The sea breeze cell initially forms over the ocean (dashed red line) and propagates both onshore and offshore (solid red line).

Bowers [38] carried out simulations of the LSB circulation off the New Jersey coast, USA, and found that wind speeds decreased from the coast to ~50 km offshore (i.e., to the divergence region; (Figure 1b) and then increased farther offshore between 70 and 100 km. The spatial extent of the sea breeze's offshore component exceeded the inland component by a factor of two or more. Wind speeds also decreased from the coast to the sea breeze front [39]. The propagation speed of the sea breeze front was rapid as it approached the coast, but decreased over the land due to friction; however, a relatively higher temperature difference near the sea breeze front and a weaker opposing surface flow also accelerated the sea breeze front [40]. Miller et al. [11] concluded that the surface friction, Coriolis force, atmospheric stability, local topography, and land–sea temperature contrast determined the inland propagation speed and extent of the sea breeze front.

Although many studies have examined the onshore characteristics of the sea breeze, few have examined the characteristics of the LSB over the ocean [19,41–43]. Steele et al. [35] reported that the behaviour and characteristics of the marine component of sea breeze cells have received little attention relative to their onshore counterparts. In fact most of the literature reports only the onshore component of the sea breeze (Figure 1a) and neglect the offshore section of the sea breeze cell (Figure 1b). From the available literature, we can deduce that the sea breeze's offshore extent varies depending on its geographical position in relation to the latitude [36,44–47]. Simpson [5] suggested that the seaward extent was comparable to the landward extent. Finkele et al. [48] found that geostrophic winds generated by the synoptic system affected the offshore extent and inland penetration speed of sea breezes in South Australia. Here, light and moderate geostrophic winds resulted in a non-uniform inland and offshore propagation with similar offshore extents, but when stronger geostrophic winds were present, the sea breeze was restricted to offshore regions. In the southern North Sea, the sea breeze's offshore extent varied with the location and timing of the divergence zones depending on the coastline orientation relative to the prevailing wind direction [35]. Analysis of scatterometer data have indicated that the offshore extent of the sea breeze could extend >300 km from the coast [36].

As the land–ocean temperature difference drives the LSB system, processes that affect the ocean temperatures, such as coastal upwelling have an influence on the LSB system [14]. Coastal upwelling also produced an earlier sea breeze onset, and a shallower, sharper, and more intense offshore/onshore sea breeze [14]. In general, coastal upwelling intensifies LSB circulation through reduced coastal ocean temperatures; however, the simulations of the LSB circulation off the New Jersey coast showed a well-developed sea breeze that was not affected by upwelling that penetrated farther inland than a sea breeze affected by upwelling [38].

The understanding of the LSB system, in particular the spatial and temporal variation in wind speed and direction is of critical importance for the development of offshore wind farms. Similarly, participants of sailing, wind and kite surfing competitions have a great interest in the direction and speed of the flow in the lowest 10–20 m above the sea surface, as well as variability during the day within the competition area that will influence the race strategy. LSB system also influences the coastal circulation and mixing. The coastal zone is the receiving basin for input of suspended and dissolved matter that includes nutrients, biota and pollutants from the terrestrial system and thus the LSB is a major influence on their dispersal.

Study Region

The study region (Figure 2), south-west coast of Australia (SWA), experiences a Mediterranean climate and is an ideal location to examine the diurnal wind effects on the local ocean circulation because of the strong, persistent LSB system. Here, during the austral spring and summer, strong and persistent LSB system is established with winds often exceeding 15 ms^{-1} [10,12,49–52]. During winter months, weak sea breezes (max speeds to 7 ms^{-1}) occur during periods between transit of fronts when high pressure systems dominate [51]. During the austral summer, the study region experiences ~20 sea breeze days per months with mean speeds 6–7 ms^{-1}. In winter ~12 sea breeze days, occur per month with mean speeds ~5 ms^{-1}. On average, 197 sea breeze days are experienced each year with a mean wind speed of 5.7 ms^{-1} [7].

The region is micro-tidal, with diurnal tides and a mean spring tidal range of ~0.6 m [52]. Semidiurnal and diurnal tidal currents at the surface represent 4–10% of the total current variance, with typical amplitudes that are ~0.02 ms^{-1} [53]. Continental shelf processes, which are mainly wind-driven and include mixing, circulation, and particulate resuspension is dominated by LSB activity, particularly during the summer months [10,12,49,51].
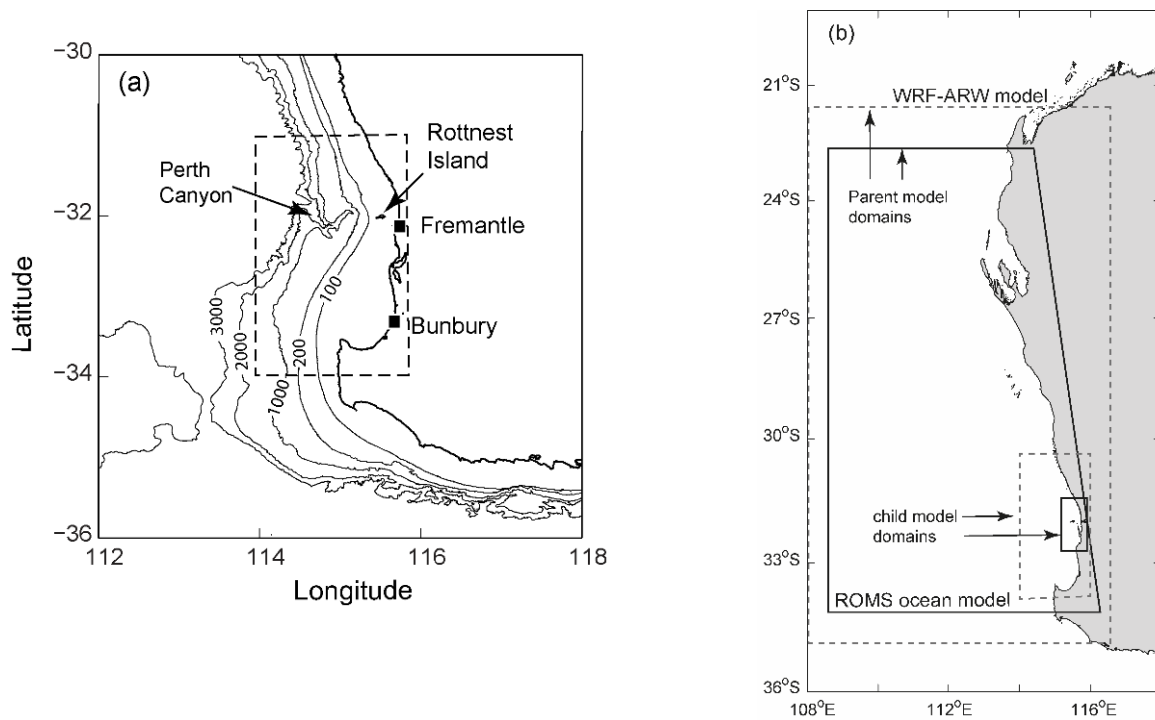
Figure 2. (**a**) Location of the study region in south-west Australia. The box identified by the dashed line shows the primary area of interest. Bathymetry is in meters; (**b**) Extent of the model grids used in the study including parent and child model domains for the WRF-ARW (dashed lines) and ROMS ocean model (solid lines).

The main bathymetric features of the study region include (Figure 2): (1) an upper continental shelf having a mean depth of 40m; (2) depth increasing rapidly in the lower continental shelf between 50m and 100m isobath; (3) the shelf break located at the ~200m isobath; (5) presence of Rottnest Island that interrupts the shore parallel flow; and, (6) the Perth canyon located to the west of Rottnest Island. The major ocean current in the study region is the warmer, Leeuwin Current (LC) that flows southward along the 200 m isobath [54–56]. On the continental shelf the Capes Current is in water depths of <50 m and transports colder water northward in summer driven by sea breeze winds [57]. The LC exhibits strong temporal and spatial variability and, of relevance to this study, is the presence of eddies in the Perth canyon due to the interaction between the LC and the local topography that includes the presence of the canyon and also the curvature of the 200 m depth contour [53].

The local LSB system typically features weak, offshore wind speeds (~5 ms^{-1}, direction ~90°–100°) in the morning, with wind speeds increasing by late morning/early afternoon because of the increasing temperature difference between the land and the ocean (Figure 3). The breeze reaches a maximum speed (10–15 ms^{-1}) by late morning/early afternoon with direction ~200° and then decreases overnight (Figure 3). Occurrence and intensity of the sea breeze in Perth is strongly related to the presence and position of the West Coast trough that is a common feature in Western Australia [58]. During the summer months, the presence of a high-pressure system to the south of Australia results in easterly airflow across the continent. The heating of this air mass as it travels across the continent results in a low-pressure trough forming in a north-south direction [59]; see also Figure 3 in [7]). This pressure trough is generally located inland of the coast, but its position is subject to day-to-day variations and when the trough lies offshore the easterly winds are strong and coastal sea breezes are delayed or non-existent. However, when the trough moves onshore easterly flow at the coast weakens, leading to the development of strong and early sea breezes. With the typical passage of weather systems from east to west, the LSB system is maintained for 7–10 days and is usually followed by a summer storm where southerly winds are encountered for periods up to 5 days prior to the re-establishment of the LSB (Figure 3).
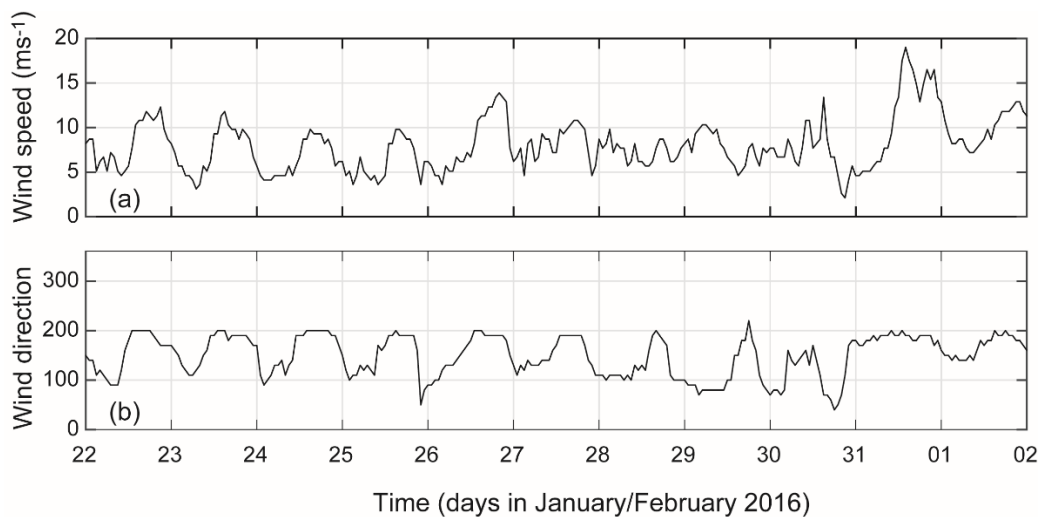
Figure 3. Time series of (**a**) wind speed; and (**b**) wind direction over the period 22 January to 1 February 2016. Data from the Rottnest Island meteorological station. The wind direction is according to the meteorological convention.

A particular feature along SWA is that the land breeze blows offshore during the night and early morning, and the afternoon breeze is obliquely-onshore i.e., south-southwesterly (Figure 3b). This is in contrast to a pure LSB system where the sea breeze blows perpendicular to the shore (onshore) in the afternoon (Figure 1). Pattiaratchi et al. [10] attributed the shore-parallel sea breeze in SWA to the interaction between the LSB system and the synoptic weather patterns. The combination of the sea breeze system (strong southwesterly airflow) and the synoptic pressure (weak northeasterly airflow) results in an obliquely-onshore (south-southwesterly) sea breezes. When the location of the west coast trough is such that the synoptic pattern induces southerly winds, the sea breeze enhances the southerly winds, resulting in very strong sea breezes with wind speeds in excess of 10 ms^{-1} (Figure 3a). Mihanović et al. [5] showed that over the diurnal cycle winds rotated in a counter clockwise (anti-cyclonic) direction.

The LSB's diel anti-clockwise rotation was transferred to the coastal currents at the surface [50]. On the inner continental shelf, in the absence of tidal forcing, the depth, magnitude, and lag times of the currents' speeds and directions varied through the water column, depending on the sea breeze intensity. For example, the correlation between the sea breeze and the currents was higher during strong sea breezes, with shorter lag times for the bottom current response [12]. The mean surface current data obtained with the HF radar revealed an almost instantaneous response of the surface currents to changes in the wind direction during sea breeze events, and a strong counter clockwise rotation, which corresponded to the wind vector's diurnal rotation [50]. The influence of the LSB on surface currents could be identified up to 140 km offshore, exceeding the coverage of the measurement region [50,53]. Edwards [60] and Lerczak et al. [61] found that the offshore extent of the sea breeze to be up to 250 km along the east and west coasts of the United States, respectively.

Many studies have examined the impacts of the LSB system in SWA; however, the LSB's time and space characteristics, particularly its evolution, frontal propagation, and offshore extent, are generally unknown. In this paper, we use field measurements together with atmospheric and ocean numerical models to examine the LSB system dynamics in and over the ocean and the surface current response in south-west Australia.

2. Materials and Methods

We use a combination of field measurements and numerical modelling to examine the LSB off south-west Australia. Both the atmosphere and ocean are considered. We examine the period January

2016 to December 2017. Majority of the numerical model data were from the summer of 2016–2017 (1–10 December 2016 and 1–28 February 2017).

2.1. Field Measurements

Meteorological data were collected at the Rottnest Island (Figure 2) meteorological station (32.0069° S, 115.5022° E), located ~25 km off the coast. Wind speed and direction were recorded 43.1 m above the sea surface every 30 min and data collected during the period 2016–2017 are presented here. These data were interpolated and re-sampled into one-hour intervals. Wind vectors are presented as the direction the wind is coming from following meteorological convention.

Surface currents obtained from shore-based HF Radar systems were available for the study region [53]. The measurements are part of the part of the Australian Integrated Marine Observing System (IMOS) and collected by the Ocean Radar facility based at The University of Western Australia. Coastal ocean surface current maps, using a high-frequency, phased array wave radar—the WEllen RAdar (WERA) were available at hourly intervals. The Rottnest Shelf WERA HF Radar system transmits at a frequency of 8.5125 MHz with a bandwidth of 33 kHz, and surface currents are derived by detecting the Doppler shift of the electromagnetic radiation's Bragg scattering over a rough sea [62]. High-frequency radar systems were first used to measure surface currents more than three decades ago [63,64] and are now widely used around the world with a high level of accuracy [65]. Detailed description on the HF Radar system installed in the study region are provided by Mihanović et al. [50] and Cosoli et al. [53] with data analysis procedures given by Cosoli et al. [66]. Briefly, the surface current vectors were derived over a regular grid with a horizontal resolution of 4 × 4 km and a maximum offshore range of around 150 km.

2.2. Numerical Models

We used output from three-dimensional, mesoscale, atmospheric and ocean models (http://coastaloceanography.org/). These models were established as a forecast system for Western Australia. The main parameters we used to analyse the LSB system were the wind vectors (10 m above mean sea level) and the surface currents. The same atmospheric and ocean model combination was used by Mahjabin et al. [67] to examine dense water transport in the study region.

The atmospheric model is the National Center for Atmospheric Research's weather research and forecasting (WRF) modelling system, WRF-ARW (Advanced Research WRF), version 3.7 [68]. The model output during typical summer conditions in 2016 and 2017 were extracted for analysis. WRF model is a mesoscale, numerical, weather prediction system designed to assist with atmospheric research and operational forecasting [68,69]. It is a fully compressible, non-hydrostatic model. Its vertical coordinate is a terrain-following, hydrostatic pressure coordinate, and its horizontal grid is an Arakawa staggered C-grid. The model uses a third-order Runge–Kutta time integration scheme [70] and second to sixth-order advection schemes for the horizontal and vertical directions.

The WRF-ARW model was configured for two domains: (1) the parent model domain, which ranged from 35° to 20° S, 107° to 117° E, with a horizontal resolution of 10 km and 45 levels in the vertical; and (2) a one-way nested child model domain for the wider Perth region, with a 2-km horizontal resolution, which ranged from 33.78° to 30.96° S, 114.31° to 116.13° E. The boundary and conditions for the parent model were Global Forecast System (GFS) model (at 0.25° resolution). Together with other meteorological parameters, the WRF-ARW model provided hourly wind speed and direction data at 10-m height from 2016. The WRF model for the higher resolution Perth regional model has been validated using field measurements from 10 coastal stations across the domain over a 2-year period [71]. For Rottnest Island the correlations coefficients (standard deviations) of 0.99 (0.78), 0.93 (2.1), 0.93 (2.1) were obtained for sea level pressure, east and north components of wind, respectively.

To simulate the oceanic currents, we used the Regional Ocean Modelling System (ROMS), which is a three-dimensional, hydrostatic, nonlinear, free surface, s-coordinate, time-splitting, finite difference, primitive equation, numerical ocean model [72,73]. A more detailed description of the model and

numerical schemes can be found on the ROMS webpage (http://www.myroms.org). The ROMS follows a free surface, terrain-following, s-coordinate system, which considers the ocean depth as vertical layers in the model and thereby reduces the error due to the estimation of vertical grids at each step. The ocean modelling system set by the University of Western Australia consisted of two one-way, nested domains: (i) the parent model domain for the wider Western Australian region at ~1.5–2.5 km horizontal resolution; and (ii) an embedded child model domain for the wider Perth region at 500-m resolution. The ROMS bathymetry data for the deep region were obtained from the GEBCO database, which was further improved with the Australian Bathymetry and topography grid [74] and LIDAR data for the coastal regions. We used a linear programming approach to smooth the final bathymetry minimally [75]. The parent domain's non-tidal boundary conditions for the free surface, temperature, salinity, and velocity were taken from the 1/12 global degree HYCOM model (http://hycom.org) and combined with nine tidal constituents for the elevation and barotropic velocities from the global barotropic tidal inverse solution, TPXO [76]. The nested child model boundaries were updated every 600s dynamically downscaling dynamics from the parent model.

We used a Flather [77] scheme for the barotropic variables in both models and a combination of Orlanski-type radiation boundary conditions with nudging for the baroclinic velocity and tracers (temperature and salinity) [78]. A multidimensional positive definite advection transport algorithm (MPDATA), which is a conservative and positive definite scheme, was used for the advection scheme in the nested model and the active tracers (temperature and salinity) and a third-order upwind scheme was used for the parent model domain [79]. We used a third-order upwind advection scheme for the baroclinic momentum in both models.

Atmospheric forcing was prescribed every hour via bulk formulation [80]. All the required variables were obtained from the locally tuned atmospheric modelling system based on the WRF-ARW model core mentioned above. The WRF-ARW model's two domains were larger than those of the ROMS model. The WRF-ARW model also used a one-way coupled mode for boundary information exchange. Here, the WRF parent and child models were initialised daily using 3 hourly boundary conditions from global NOAA/NCEP Global Forecast System (GFS) Atmospheric Model at full horizontal (at 0.25°) and vertical resolution. Original grib2 data were pre-processed using WRF-WPS package in order to provide required WRF initial and boundary netCDF files that included vertical profiles of pressure, winds, humidity, temperature, among others. The atmosphere and ocean model outputs were saved hourly and served through an OPeNDAP THREDDS server.

2.3. Analysis Techniques

The wind components (east-west and north-south) time series from the Rottnest Island at hourly intervals were subjected to Fourier analysis to identify the dominant frequencies in the records and their variability with time. The power spectra were used to construct time frequency plots and determine the temporal variation in spectral energy distribution. A similar approach was undertaken by Pattiaratchi and Wijeratne [81] in the analysis of sea level records. Here, time series of 512 points (~20.5 days) were used to estimate power spectra using the 'Welch' method using the Fast Fourier Transform (FFT) method. Subsequent spectra were calculated using a 50% overlap (i.e., 256 points).

Wind component time series was subjected to a 33 h cut-off, Butterworth filter to separate the time series into high and low frequency components. This allowed for the examination of the high-frequency signal (i.e., the sea breeze) close to the diurnal band.

Complex demodulation [82] was used to obtain the clockwise and counter clockwise phases and amplitudes wind and surface currents from WRF and ROMS model outputs. Here, we used 15–35 h, band-passed-filtered winds and currents to extract the phases and amplitudes of the 24 h harmonics [83]. Two diurnal periods of 48 h were overlapped and slid in time with six-hour time steps [50,82]. The WRF and ROMS model outputs subjected to this analysis were used to estimate the diurnal ellipse characteristics [82].

Rotary energy spectra were calculated for the wind and surface current vectors for February 2017 following Gonella [84] and using the Fast Fourier Transform (FFT) method.

To identify the location and propagation of the sea breeze front (SBF) the east-west component of the wind from the WRF model was used and two different methods were tested: (1) we calculated the wind gradient for the cross-shore components over two successive time steps. The time variability of this gradient value over the daily cycle was determined for the study region. The SBF was identified by the discontinuity in the gradient. However, only the onshore propagation of the SBF could be identified following this method. The offshore propagating front was not associated with a strong horizontal gradient in wind as the spatial changes were more gradually in the offshore direction; and, (2) for each time step, the cell furthest from coastline in both onshore and offshore directions that was associated with a positive cross-shore (i.e., onshore) wind component was identified to be the location of sea breeze initiation. The contour line connecting these cells indicated the edge of sea breeze region associated with the change of wind in the onshore direction. This process was repeated to define the sea breeze fronts over time.

3. Results

### 3.1. Measurements: Rottnest Island Meteorological Station

Rottnest Island meteorological station, located on an island ~20 km from the land mass (Figure 2), provided an ideal data set to examine the characteristics of the sea breeze in the offshore region. The station was established in 1879 and was upgraded in 1995 as an automatic weather station. In this paper, we examine data collected over the period 2016–2017.

Time frequency diagram for the 2-year period indicated the dominance of diurnal energy, in both east and north components of wind between 1 October and 1 April (Figure 4). This period covered late austral spring, summer and early autumn periods and indicated the periods when the seabreeze is dominant (see also [50]). The higher energy contained in wind components for periods >24 h between April and September, represent the passage of winter fronts (Figure 4).
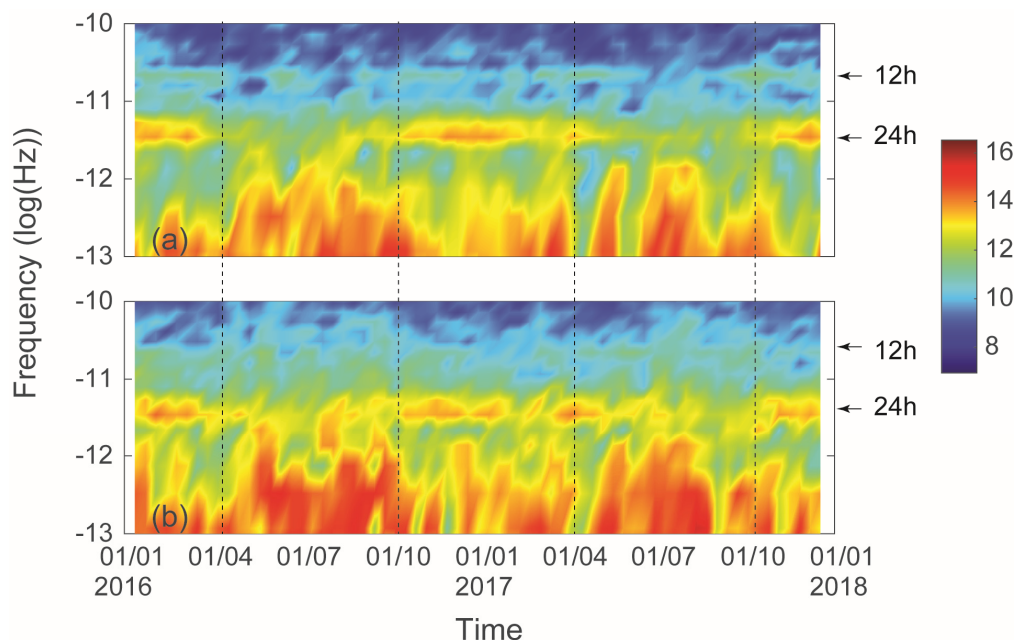
Figure 4. Time frequency plot of spectral energy calculated from the wind time series at Rottnest Island station for the period 2016-2017. (**a**) east-west component; and, (**b**) north-south component. Units of spectral energy are log[m^{2}s^{-2}/Hz].

Time series of the meteorological data for January 2016 highlighted the LSB system (Figure 5). All of the parameters indicated a diurnal variability except for sea level pressure (SLP) that has a semi-diurnal variability. There was also a low frequency change of O(10) days that is related to the passage of high pressure systems across the study region. The diurnal changes in wind speed during the sea breeze cycle reflected changes in SLP. The two daily maxima in SLP corresponded to minima in wind speed in the morning and the beginning of the decrease in wind in the afternoon. (Figure 5a,e). Usually, there was a decrease in air temperature when the wind speed increased explaining the local term 'Fremantle Doctor', cooling afternoon sea breeze that brings respite from the usually hot weather. Note that the higher maximum temperatures were experienced when the afternoon winds were weak and/or variable in direction (e.g., 7–8 and 14–15 January).
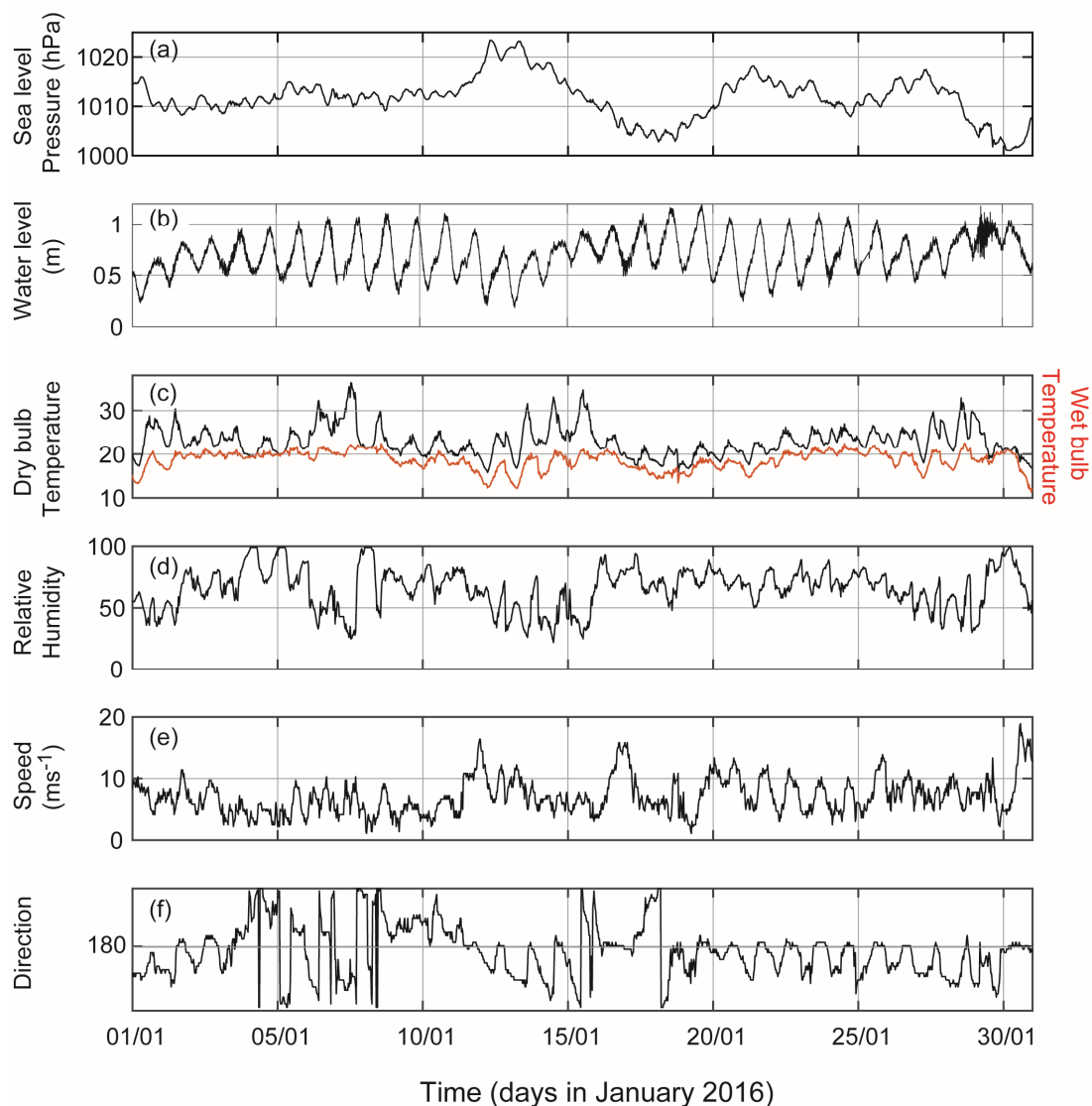
Figure 5. Time series meteorological parameters and water level in January 2016 from Rottnest meteorological station: (**a**) mean sea level pressure; (**b**) water level at Hillarys boat harbour relative to Australian Height Datum (AHD); (**c**) dry and wet bulb temperature; (**d**) humidity; (**e**) wind speed; and, (**f**) wind direction. Meteorological convention is used for wind direction.
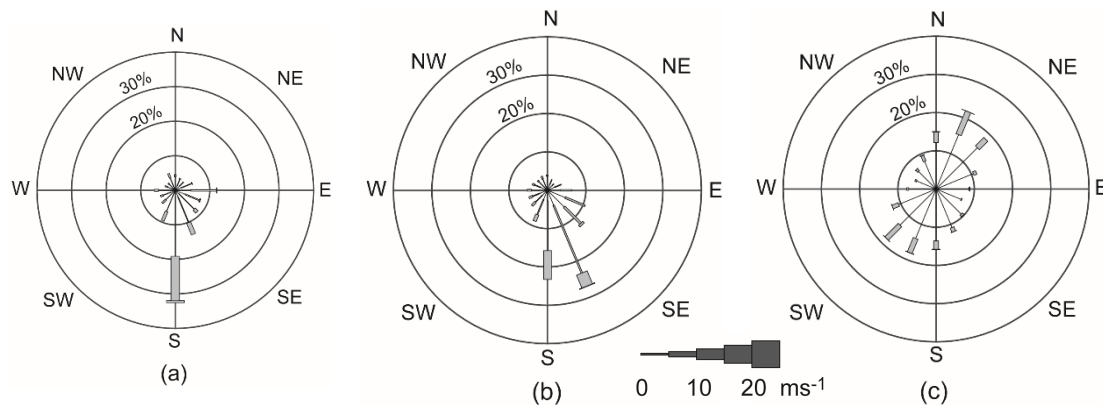
The mean hourly time series for the period 22–30 January 2016 when consistent sea breeze cycles were experienced (Figure 3), indicated the diurnal cycle of the sea breeze (Figure 6). The wind speed decreased between midnight and 0400 and was relatively constant to 1100, increasing rapidly to a maxima of ~10 ms^{-1} at 1800 and decreasing to midnight (Figure 6a). The wind direction reflected the

changes in wind speed with the winds blowing from south-east (120°) and shifting to almost southerly (~200°) when the winds were strongest (Figure 6b). Note that the wind direction started to change ~0900 before the wind speed increased. The hodograph of mean hourly wind speed and direction, with synoptic winds removed, indicated an orientation south-west to north-east and an anti-clockwise rotation (Figure 6c).
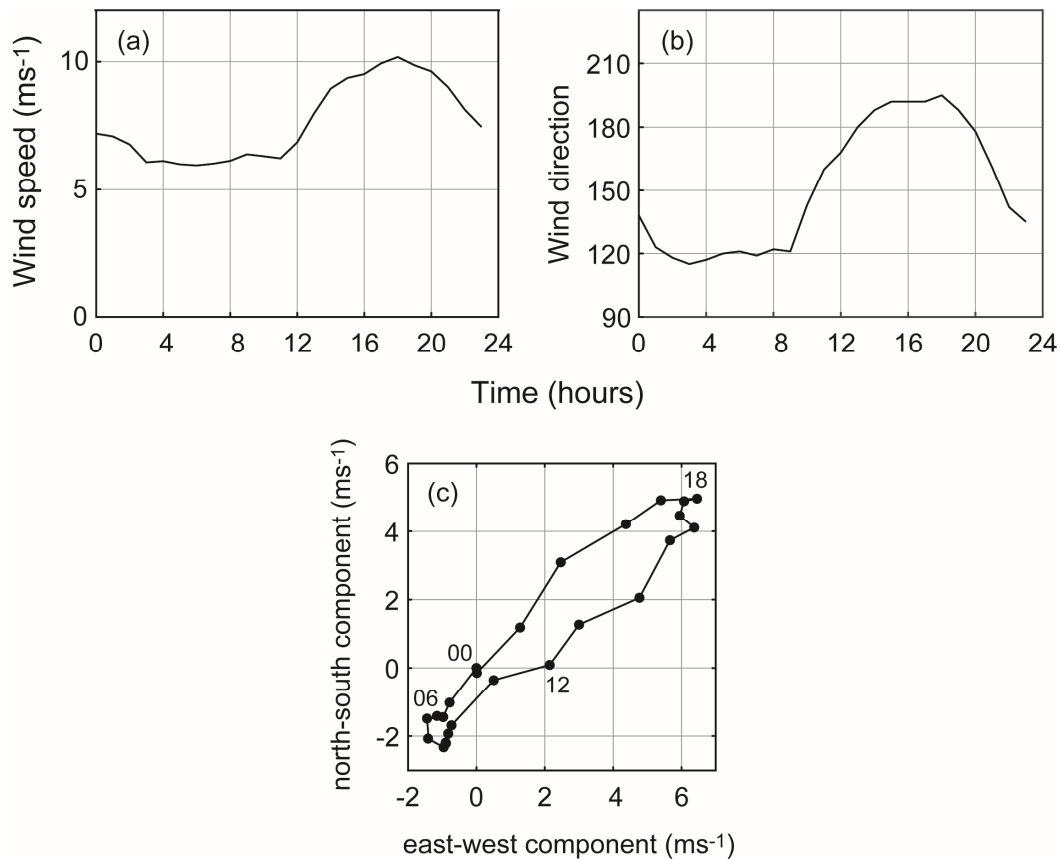
Figure 6. Time series of mean (**a**) wind speed; and, (**b**) wind direction for the period 22–30 January 2016. (**c**) hodograph plots of (**a,b**) with synoptic winds removed. The numbers on the hodograph represent local time in hours. Data Rottnest meteorological station.

Decomposition of the wind time series using a 33-h, Butterworth filter to high and low frequency components revealed the LSB and the synoptic system components (Figure 7). Here, the low-passed (periods > ~40 h) and high-passed time series (periods < ~28 h) represented the synoptic and LSB system, respectively. The wind rose for the original data record (22 January to 1 February 2016) indicated a dominance of southerly winds (Figure 7a). The low-pass time series indicated winds mainly from the south and south-south-east (Figure 7b) that represent the synoptic winds associated with a high-pressure system located to the south of Australia [7,10]. The wind rose for the high-frequency component showed winds aligned to a south-west to north-east axis, oriented ~45° counter clockwise from the east and represented the LSB system.

**Figure 7.** Wind roses for (**a**) original time series; (**b**) low pass time series; and (**c**) high pass time series for the period 22 January to 1 February 2016. Data from the Rottnest Island meteorological station. The wind direction is according to the meteorological convention.

3.2. WRF Model Output

Rottnest Island station provided meteorological data from a single point over time but did not contain any information on the spatial variability of the sea breeze within the study region. The WRF model output was used to fill in this gap to examine the spatial variability but also the output was used to determine the expansion of the sea breeze cell (Figure 1b) with time.

Time series of the spatial distribution wind vectors for the study region during two typical sea breeze cycles (on 8 December 2016 and 23 February 2017) are shown on Figures 8 and 9. The time and spatial variability of the images indicated that in the morning (0800), the winds across the whole region were offshore (easterly), representing the land breeze (Figures 8a and 9a). There were also east-west bands of low winds, the largest at 33.0° S where the sea breeze cell (SBC) was beginning to form. At 1000 winds on land and further offshore were easterly whilst there was a band of weaker winds with variable direction adjacent to the coast (Figures 8b and 9b). The SBC had expanded onshore, offshore and alongshore. In the region between latitudes 32.5° S and 33.0° S the winds were relatively stronger (~5 ms^{-1}) and had a southerly component, the sea breeze. By 12 noon, the winds over the ocean had a southerly component whilst inland, the winds were still easterly (Figures 8c and 9c). Closer to the coast, the winds increased in speed (~8 ms^{-1}) and were south-westerly. Inland penetration of the sea breeze started in the mid-section of the study region (Figures 8c and 9c). At 1400, wind speeds continued to increase, southerly winds were present offshore, inland penetration of the sea breeze continued with winds oriented from south-west on land (Figures 8d and 9d). By 1600, wind speeds over the ocean were >10 ms^{-1}. On the ocean and to the north of Rottnest Island (Figure 2) the winds were southerly whilst to the south of Rottnest Island winds were south-westerly (Figures 8e and 9e). At 1800, wind speeds reached a maximum over the ocean (Figures 8f and 9f) as reflected in the Rottnest Island measurements (Figure 6a) with similar directions as at 1600.
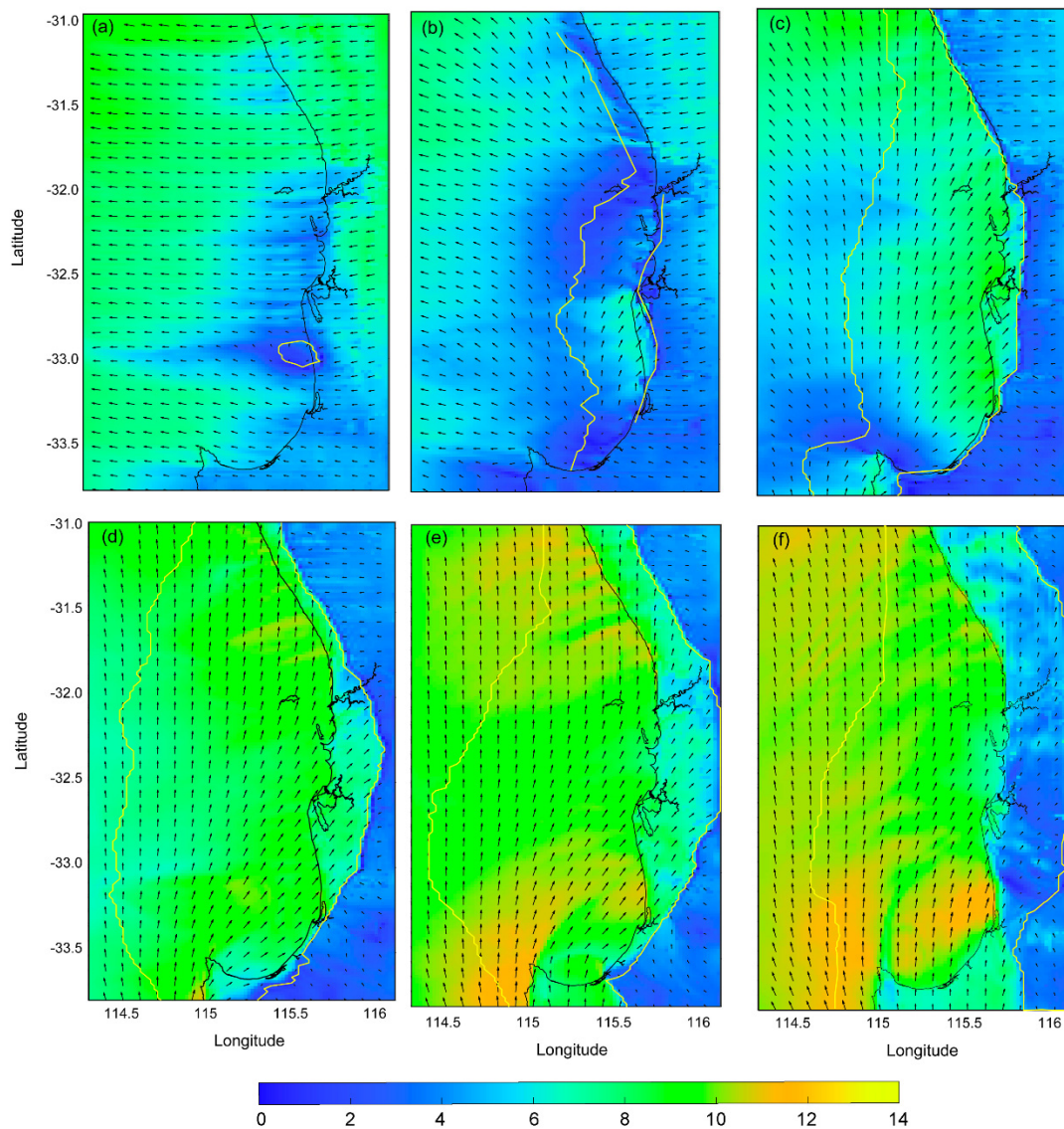
Figure 8. Time series (two-hourly intervals) of the spatial distribution wind vectors for south-west Australia during a typical sea breeze cycle predicted from the WRF model on 8 December 2016. (**a**) 0800; (**b**) 1000; (**c**) 1200; (**d**) 1400; (**e**) 1600; and (**f**) 1800. The contour outline of the sea breeze cell is shown by the yellow line. The colours represent wind speed in ms^{-1}.

The spatial distribution of wind vectors with time also allowed for the determination of the characteristics of the sea breeze cell (SBC) and its evolution with time (Figures 8 and 9). Note that as the LSB system evolved, there were two fronts that propagated inshore and offshore, respectively (Figure 1). In the study area, the SBC was consistently initiated close to the coast at ~33° S where a region of weak and variable winds was present and the SBC could be identified from the cross-shore velocity component analysis (Figures 8a and 9a). With time, the SBC was oriented parallel to the coast and propagated both offshore and inland (Figures 8b–f and 9b–f). Divergence of the wind velocity vectors with time identified the location of the SBF onshore on both days but due to weaker velocity gradients in the offshore direction the SBF was not defined from this method (Figure 10). However, the divergence method identified the initial location of the SBC to be near the coast ~33° S.
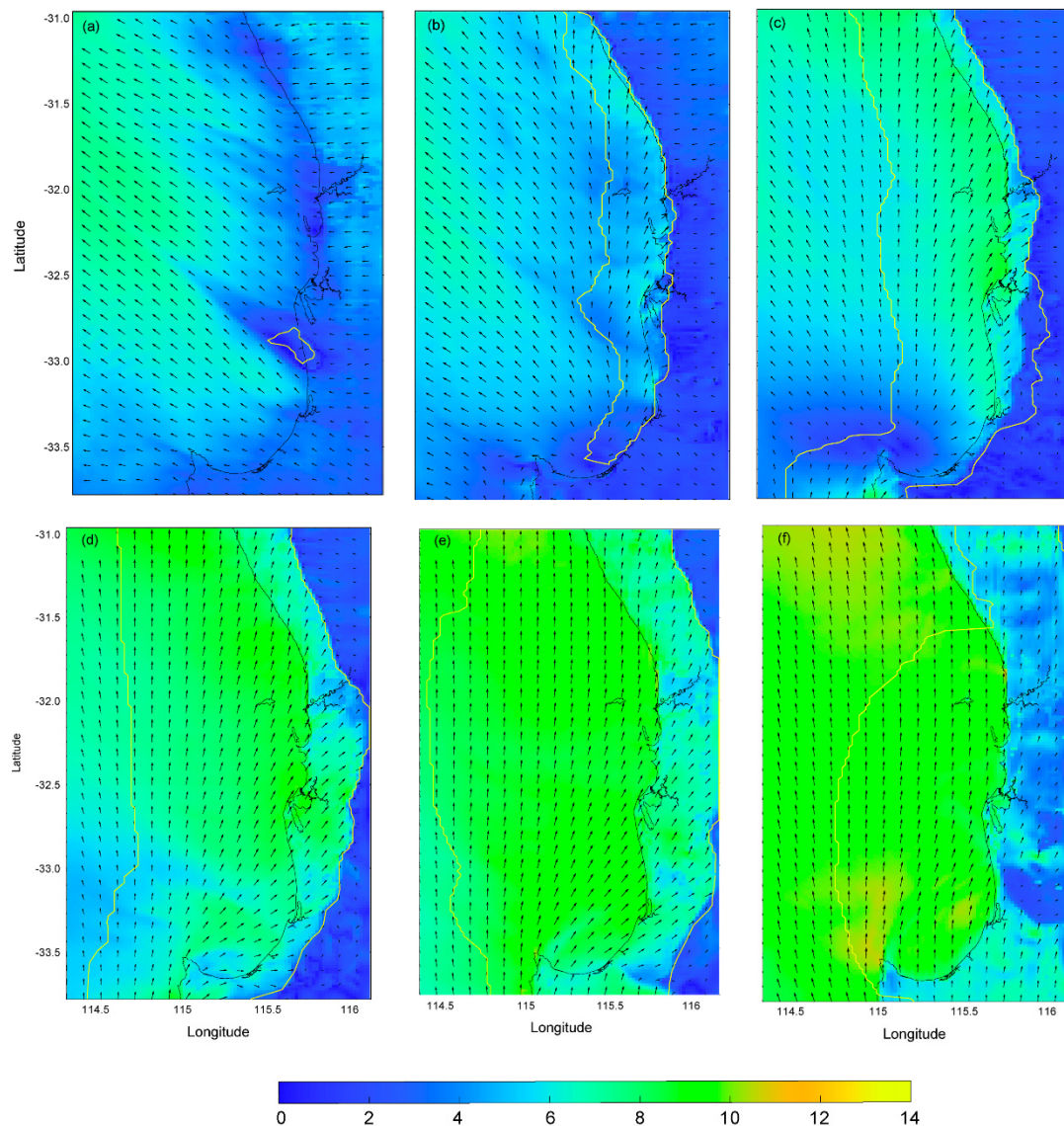
Figure 9. Time series (two-hourly intervals) of the spatial distribution wind vectors for south-west Australia during a typical sea breeze cycle predicted from the WRF model on 23 February 2017. (**a**) 0800; (**b**) 1000; (**c**) 1200; (**d**) 1400; (**e**) 1600; and (**f**) 1800. The contour outline of the sea breeze cell is shown by the yellow line. The colours represent wind speed in ms^{-1}.

The propagation speed in the offshore direction was rapid compared to its propagation speed inland mostly due to increased friction on the land surface. The evolution of the mean location of the SBC at hourly intervals, obtained by averaging ten sea breeze cycles (1–10 December 2016) reflected these observations for a typical day (Figure 11): the SBF was initiated close to the coast at ~33° S, around 0800 and propagated both offshore and onshore, and at the same expanding in an alongshore direction. The SBF reached the maximum offshore extent at 1600 and was 120–150 km from the coast. In comparison, the maximum onshore propagation was ~30–40 km but was constrained by the eastern boundary of the model (e.g., Figures 8f and 9f). The mean onshore and offshore SBF propagation speeds indicated that both increased linearly, reaching maximum speeds by 1100 and then decreasing (Figure 12). However, there were large differences in the propagation speeds in each direction. The offshore propagation speed increased from 13 to 30 kmh^{-1} between 0700 and 1100 whilst the onshore propagation speeds increased from 5 to 9.5 kmh^{-1} over the same time period. The maximum offshore propagation speed was a factor 3 higher than the onshore propagation speed (Figure 13).
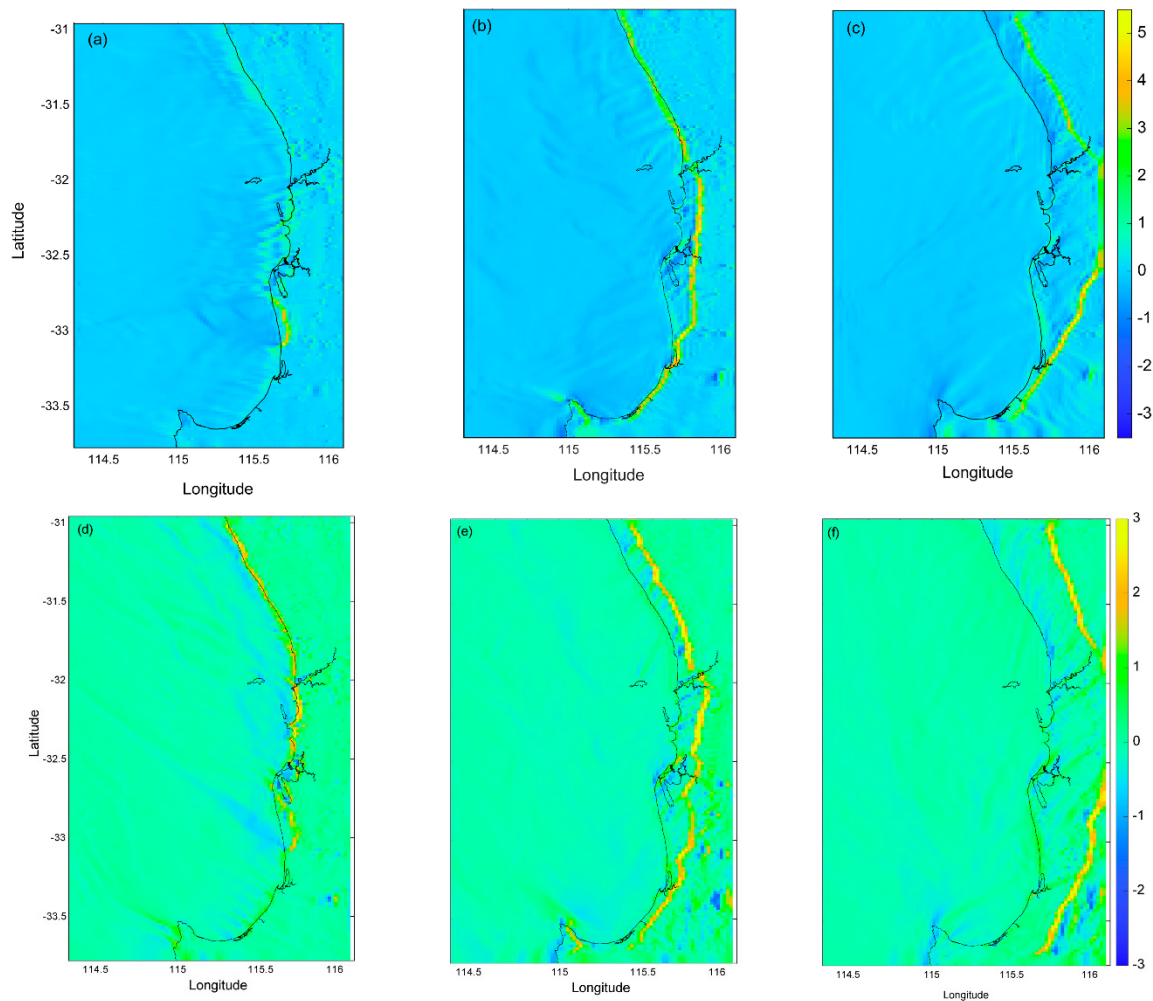
Figure 10. Divergence of the wind vector: (**a**) 0900; (**b**) 1200; and, (**c**) 1500 for 8 December 2016 (same as that for Figure 8); and, (**d**) 0900; (**e**) 1200; and (**f**) 1500 for 23 February 2017 (same as that for Figure 9). Units of divergence are s^{-1}. Note different scales for the different days.
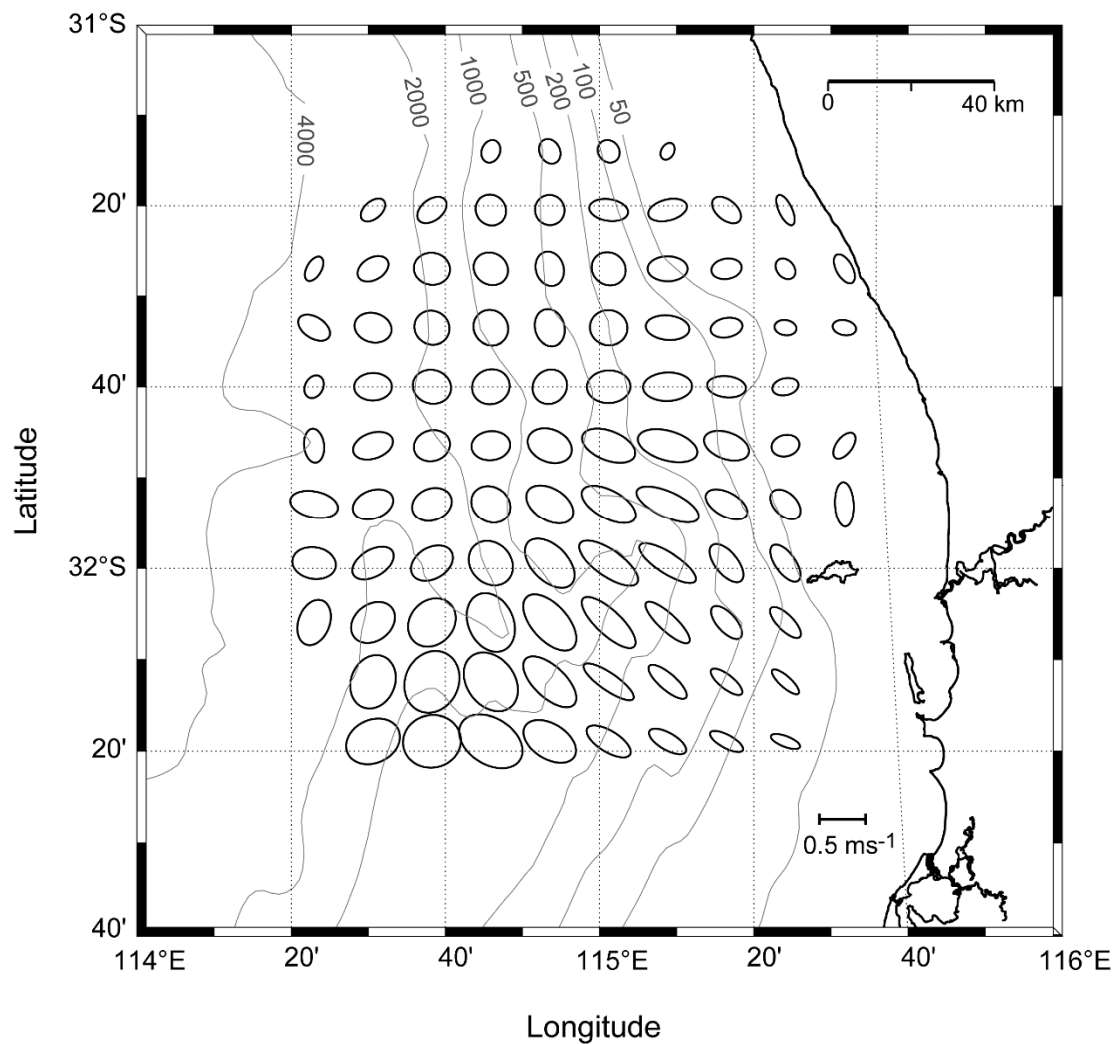
3.3. Surface Currents from HF Radar

The diurnal surface current ellipses calculated using the HF Radar data during February 2017 indicated circular motion in the deeper water whilst on the continental shelf region in water depths <200 m, the circulation was less circular (Figure 13). Surface currents rotated counter clockwise across the whole region. The current amplitudes were up to a factor 5 larger in the deeper regions compared to those on the continental shelf (Figure 13). These results are the same as that reported by Mihanović et al. [50] for the same region with data collected in February 2011. The strong diurnal currents are generated through a resonance mechanism resulting from the sea breeze forcing period of ~24 h being close to the local inertial period [50].
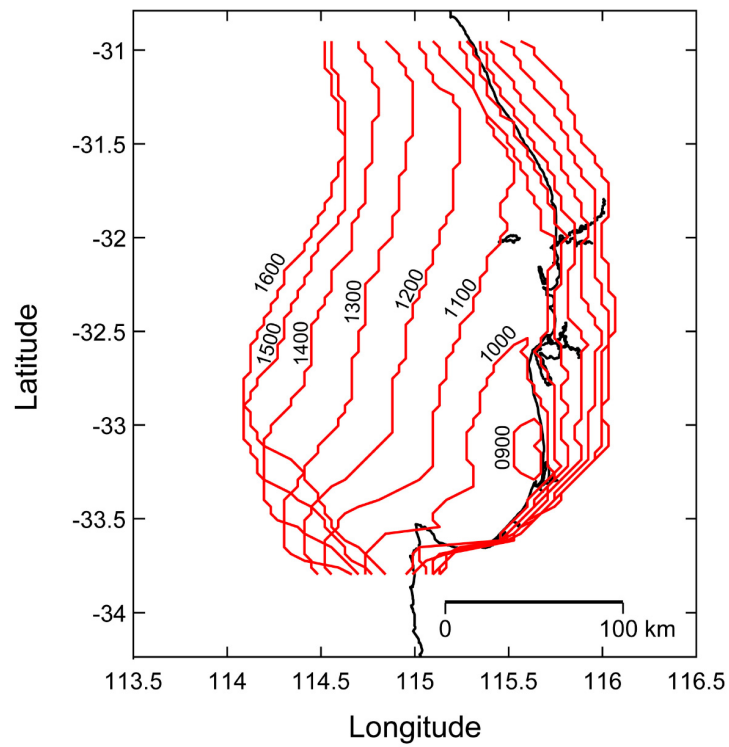
Figure 11. Time variability of sea breeze cell locations at hourly intervals from 0900 to 1600 averaged over a 10-day cycle (1–10 December 2016).
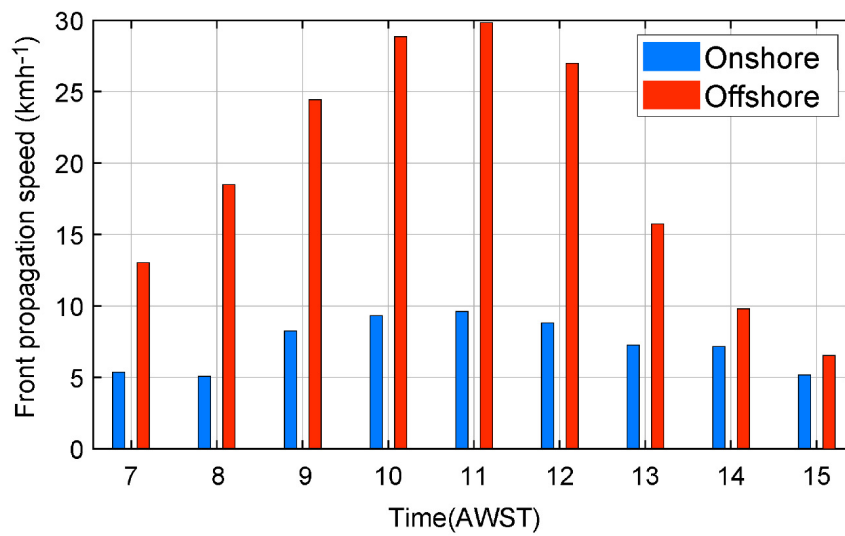

Figure 12. Time variability in mean propagation speeds of the sea breeze fronts onshore (blue) and offshore (red). Means were obtained over a 10-day cycle (1–10 December 2016).

Figure 13. Diurnal surface current ellipses calculated from data collected in February 2017. For clarity, current ellipses denote every third HF Radar observation point that had at least two-thirds of temporal coverage in February 2017. All ellipses rotated anti-clockwise.

3.4. ROMS Model Output 4

Three hourly predicted surface currents from the ROMS model for 8 December 2016 indicated the typical response to sea breeze wind forcing of the currents (Figure 14). The LSB cycle on this day, used to force the ocean model, was very similar to the mean wind pattern (Figure 6) with south-easterly (120°) winds in the morning and almost southerly (200–210°) winds in the afternoon. The wind speed started to increase after 12 noon reaching a maximum of 10 ms^{-1} around 1800 (Figure 6). The surface current response was influenced by the local topography (Figure 2): (1) presence of Rottnest Island that imposes a barrier to the surface currents between the southern and northern regions; (2) deeper water (>100 m) to the west of Rottnest Island associated with the start of the Perth canyon; and, (3) the shallower inner continental shelf where the water depths <50 m (this is the region east of 115° E, approximately shoreward of Rottnest Island).
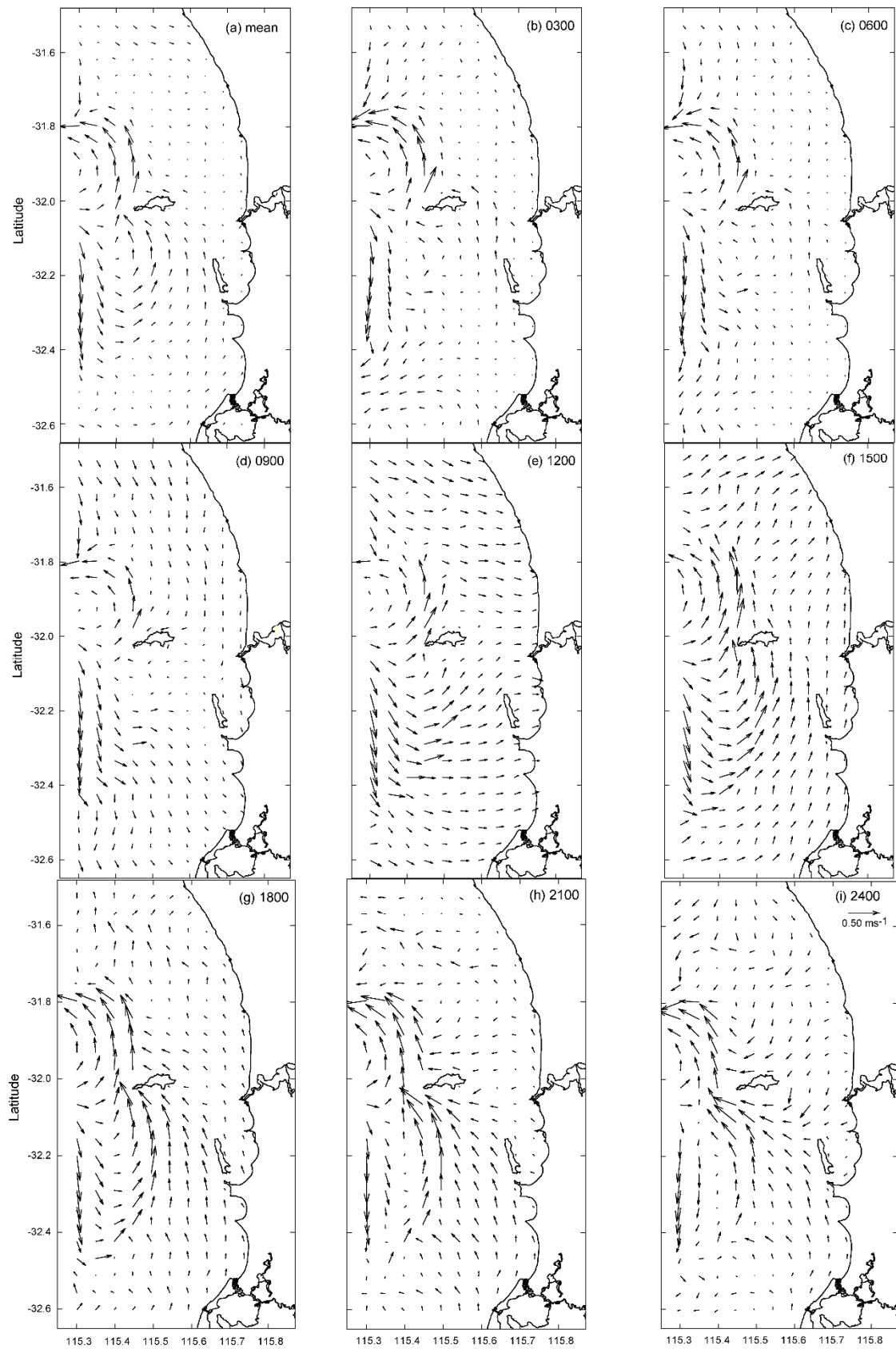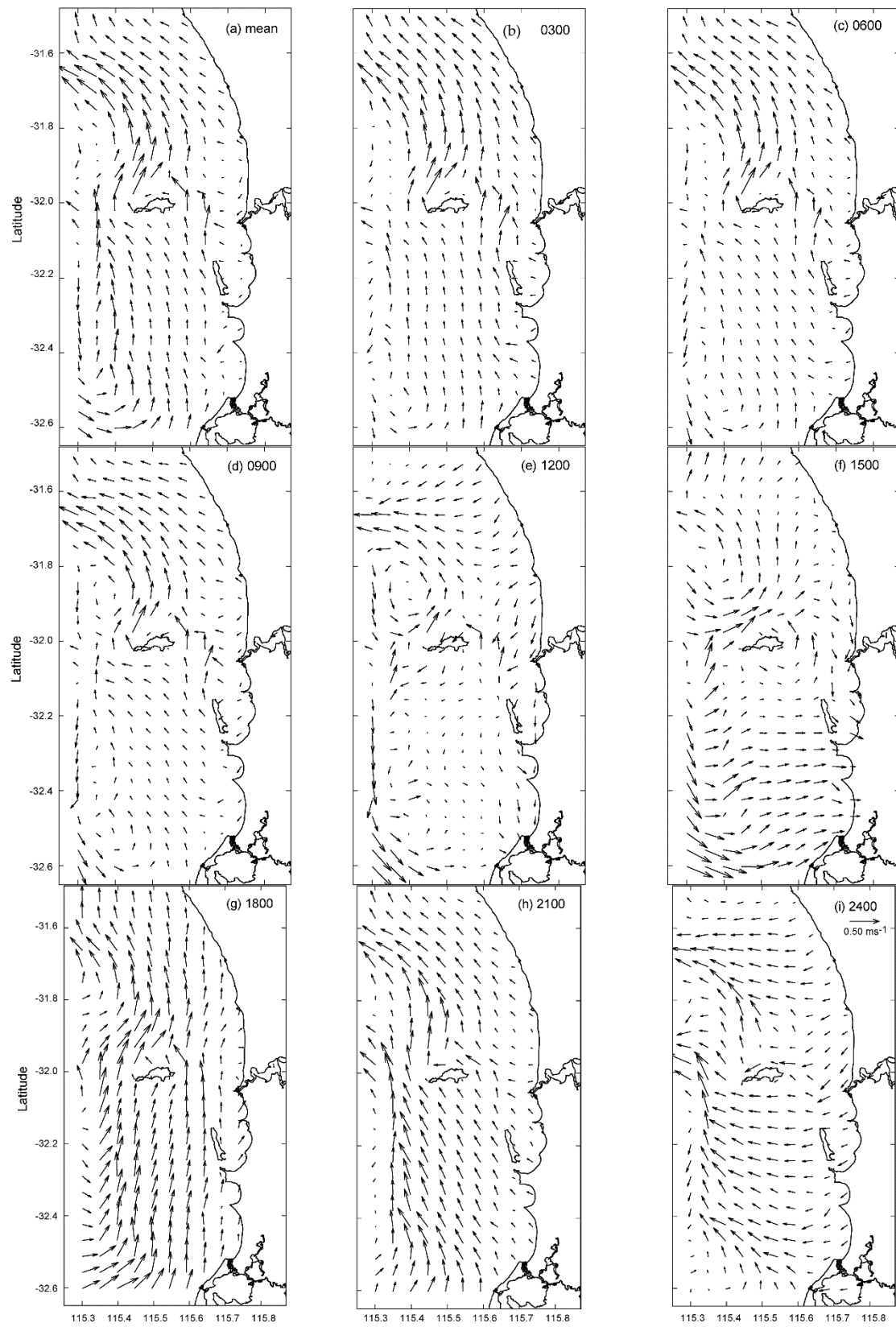
Figure 14. Surface ocean currents in the study region over a diurnal cycle on 8 December 2016 from the ROMS model. (**a**) mean over 24 h; and (**b**–**i**) current vectors at 3 hourly intervals. Note the velocity scale for all plots are shown on (**i**).

The mean currents over the 24 h period (Figure 14a) indicated inflow of water into the model domain, to the west of Rottnest Island, associated with the deeper water (Perth canyon; Figures 2 and 13). This onshore stream of water bifurcated and flowed both to the north and south (Figure 14a). The southward stream recirculated to the north and flowed past the western tip of Rottnest Island (Figure 14a). The northward arm of the inflow, augmented by flow past the island moved north and exited the domain at 31.8° S. The mean northward currents to the south of Rottnest Island were stronger than those to the north of the Island (Figure 14a).

Over the diurnal cycle, there were no major changes in the current's patterns over the period 0300 and 0900 with similar features to the mean (Figure 14a–d). At 0900 the currents to the north of Rottnest were flowing southward and then progressively rotated anti-clockwise to be directed to the northwest by 1500 (Figure 14d–f) and the rotation completed by 2400 with the currents flowing southward. This rotation is due to the resonance between the sea breeze and the local inertial period [50]. To the south of the Island, the strongest currents were predicted from 1500 to 2100 reflecting the wind profile (Figure 6a). The northward arm of the re-circulation of water entering the domain progressively became stronger (Figure 14d–f) and then reduced in speed by midnight (Figure 14i).

The anti-clockwise eddy, located to the north-west of Rottnest Island was present throughout the day but there were changes to the structure over the LSB cycle (Figure 14). Initially (0300), the eddy is quite well defined during the morning (Figure 14b–d) under weaker south-easterly winds (note that only part of the eddy is present in the high resolution ROMS domain; Section 2.2). With the onset of the sea breeze, current speeds within the eddy increased (Figure 14e). As the winds strengthened during the afternoon, water flow moving northwards past Rottnest Island enhanced the eddy (Figure 14f–i).

Three hourly predicted surface currents from the ROMS model for 23 February 2017 over a sea breeze cycle indicated a similar response (Figure 15). The LSB cycle on this day was very similar to the mean wind pattern shown on Figure 6 with south-easterly (120°) winds in the morning and almost southerly (200–210°) winds in the afternoon. The maximum wind speeds on this day were higher at 15 ms^{-1} and followed a strong sea breeze the previous day. The surface currents were affected by the local topography (see above). However, the surface currents, directed to the north, were generally stronger reflecting the stronger LSB (Figure 9). The mean currents over the 24 h period (Figure 14a) indicated inflow from south to north flowing past Rottnest Island with stronger currents to the north of the Island. Over the diurnal cycle, there were no major changes in the current's patterns over the period 0300 and 0900 with similar features to the mean (Figure 15a–d). At 0900 the currents were flowing northward, and an anti-clockwise eddy was forming to the north-west of Rottnest Island that became progressively got stronger by 1500 (Figure 15d–f). Currents were weaker and more variable to the south of the Island with west to east flow by 1500 (Figure 15d–f). The currents across the domain were flowing to the north from 1800–2100 (Figure 15g,h) in response to the strong sea breeze and then offshore by midnight when the land breeze was established (Figure 15i).

Figure 15. Surface ocean currents in the study region over a diurnal cycle on 23 February 2017 from the ROMS model. (**a**) mean over 24 h; and (**b**–**i**) current vectors at 3 hourly intervals. Note the velocity scale for all plots are shown on (**i**).

*3.5. Diurnal Ellipse Characteristics from WRF and ROMS Models*

Field measurements of both wind and surface current vectors indicated anti-clockwise rotation over a diurnal cycle (Figures 6c and 13) and were reproduced in both atmospheric (WRF) and hydrodynamic (ROMS) models (Figure 16). Ellipse characteristics of the wind vectors were calculated over a period of one month (February 2017) and indicated that across the whole domain the semi-major axis was oriented along the southwest to northeast axis (Figure 16a). In deeper water, offshore of 115° E, the eccentricity (ratio of semi-major to semi-minor axes) of the ellipse was smaller reflecting a more circular rotation compared to that closer to the shore where the effects of the land may have a greater influence. There were also slight changes in the orientation of the major axis of the wind ellipse that were different to the north and south of Rottnest Island: to the north the axis was rotated anti-clockwise closer to the coast whilst to the south was rotated clockwise closer to the coast (Figure 16a).
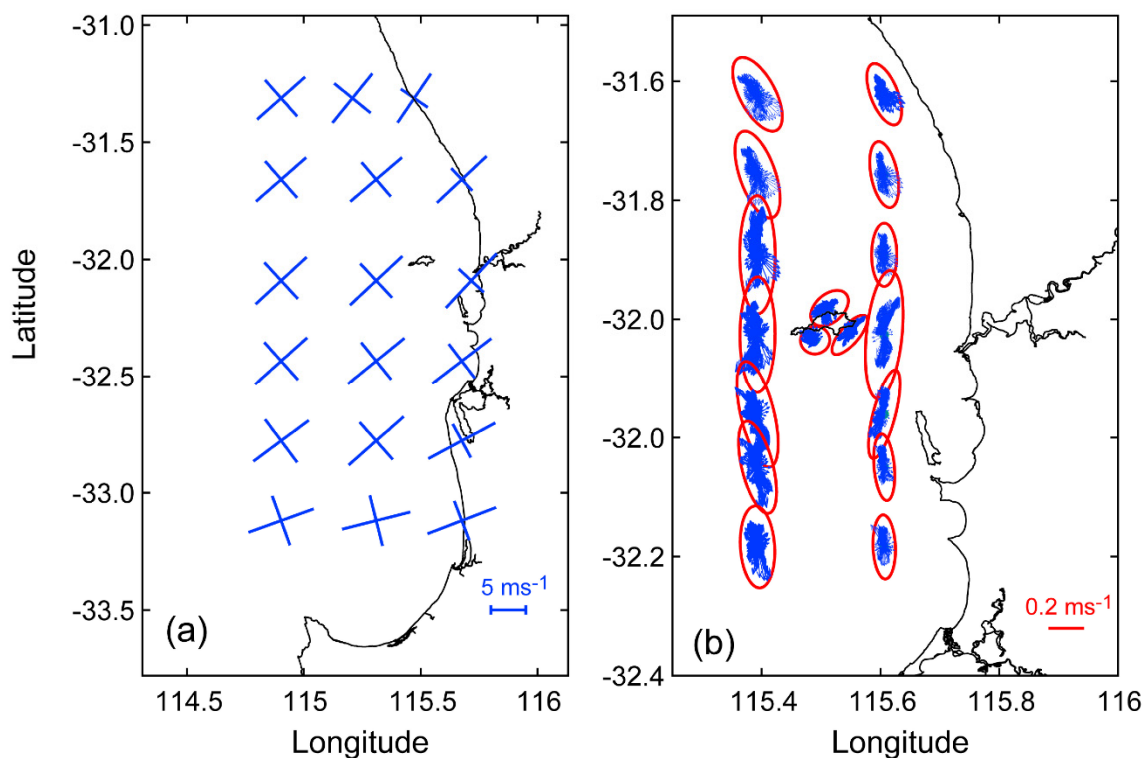
Figure 16. Ellipses calculated using numerical models: (**a**) Wind from the WRF model; and (**b**) surface currents from the ROMS model. Ellipses were calculated over a one-month period in February 2017.

The current ellipses also indicated anticlockwise rotation; however, the major axes were oriented parallel to the coast (Figure 16b) as it acts as a barrier to cross-shelf flow. The currents were generally stronger offshore compared to those closer to the coast.

Rotary energy spectra for the diurnal band indicated higher spectral energy in the anti-clockwise component compared to the clockwise component for both wind and surface currents (Figure 17). The study region is close to the 30° S where oscillations close to the inertial period are amplified through resonance between the diurnal and inertial frequencies where diurnal winds force enhanced anti-cyclonic rotary motions that contribute to near-inertial energy [50,85] and are reflected in the results. The strongest anti-clockwise energy in the wind was at the centre of the model domain close to the origin of the sea breeze front (Figures 8 and 17a). Higher clockwise energy was present over the land and to the north of Rottnest Island (Figure 17b). Anti-clockwise energy in the surface currents was enhanced in water depths > 50 m (Figure 17c), reflecting the depth influence on the inertial oscillations. The same feature is reflected in the HFR currents (Figure 13). In contrast, clockwise energy in the surface currents were weaker across the whole domain (Figure 17d).
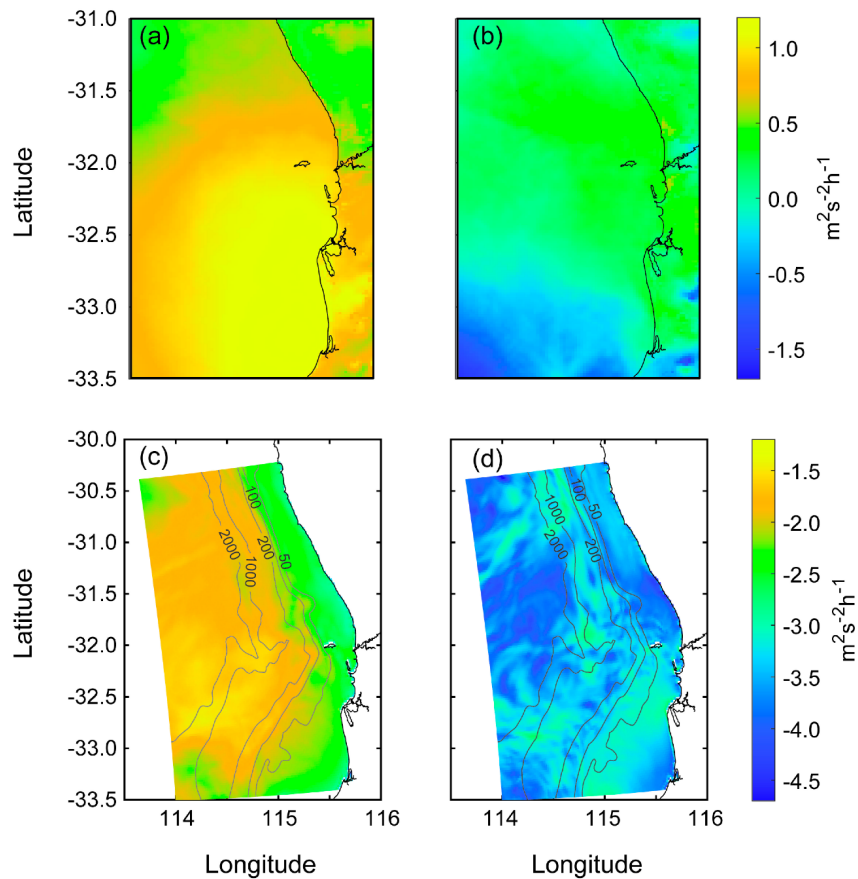
Figure 17. Diurnal energy in the anti-clockwise and clockwise components of (**a**), (**b**) wind from WRF model; and (**c**,**d**) surface currents from ROMS model. Spectra were calculated over a one-month period in February 2017.

4. Discussion

The land–sea breeze (LSB) system is one of the most intensely studied meso-scale meteorological phenomena globally over the past few centuries and as a consequence the onshore structure and physics of the LSB is well known [6,19,35,37]. A large proportion of the global population, including mega-cities are located close to the ocean and impacted by the LSB system representing a major component of the coastal wind climate. The concerns associated with air quality have resulted in many of these studies to examine issues associated with forecasting the physics and chemistry of the LSB [6,35]. In contrast, the LSB system offshore has received very little attention. Only a handful of studies have considered that there is a SBC propagating offshore. Therefore, information on frontal propagation speeds, their variation over a SB cycle and the offshore extent has not been defined. It is acknowledged that this would be site specific but with increasing interest in offshore wind farms there is renewed interest as well as for recreational use [35,86]. This study was based in south-west Australia where one of world's strongest sea breezes systems occurs with maximum wind speeds often exceeding 15 ms^{-1} during the austral spring, summer, and early autumn (October–April). The entire coastline of Western Australia was identified by Gille et al. [36] as one of the global hotspots for diurnal winds (see also [7]). The study region is located at 32° S where the inertial period is close to 24 h that results in a resonance condition between sea breeze forcing and ocean response resulting in stronger diurnal currents through the water column up to 300 m water depth [50].

The local mean LSB characteristics were such that wind speeds decreased between midnight and 0400 and were relatively constant to 1100 and increased rapidly to maxima >10 ms^{-1} (~1800) and decreased to midnight (Figure 6a). The wind direction in the morning was from south-east (120°) changing to almost southerly (~200°) when the winds were strongest (Figure 6b). The hodograph

of mean hourly wind speed and direction indicated an orientation south-west to north-east and an anti-clockwise rotation (Figure 6c). The atmospheric numerical model (WRF) output confirmed this orientation and anti-clockwise rotation and in the offshore region (Figures 16a and 17a). The anti-clockwise rotation of the winds is typical for the southern hemisphere [36].

A feature of the LSB system in the study region is that it blows obliquely-onshore (i.e., south-southwesterly) in contrast to the classic sea breeze, which blows perpendicular to the shoreline [5]. In fact, so-called 'pure' sea breezes, i.e., sea breezes that are not interacting with geostrophic winds are virtually non-existent or much weaker if they do occur, along the Perth coastline [7]. The reason for the obliquely-onshore sea breeze system in Perth was attributed to the interaction between the sea breeze and the geostrophic winds associated with the synoptic weather patterns [7,10]. Decomposition of the wind record to the diurnal and synoptic components can be used to explain the reasons for the obliquely-onshore winds in the afternoon. The diurnal component of the winds was oriented south-west to north-east (Figures 7c and 16a). However, the stronger synoptic winds were from the south-east to south (Figure 7b) and in combination the winds have a strong southerly component (Figure 7a).

Many of the previous studies, using either field measurements and/or numerical simulations, have examined the onshore propagation of the sea breeze [5,6,19,86]. Very few have examined the sea breeze cell in the offshore region (Figure 1b). This is because historically there was more interest in the onshore propagation of the sea breeze as it directly affected human populations (e.g., air quality, [6]). Additionally, measurements in the offshore regions are scarce due to high costs and difficulties in maintaining moorings and only a few studies have reported offshore sea breeze measurements [5,14,87]. In the convectional theory of the sea breeze (Figure 1b) there is onshore convergence at the sea breeze front on land, rising air, and in the offshore sinking air and divergence region that define the offshore extent (Figure 1b and [14]). The offshore divergence region may not be as clearly defined as the convergence region of the sea breeze front propagation onshore [14,35,37]. In our simulations, the sea breeze cell (SBC) was initiated ~0800 with width ~25 km straddling the ocean and the coast at 115.5° E; 33° S (Figures 8a and 9a). Although results for two days are shown (8 December 2016 and 23 February 2017), this pattern was present on almost all of the simulations. The SBC progressively expanded onshore, alongshore and offshore, reaching a total (offshore to inshore) width of ~150 km after 8 h (Figures 8e and 9e). This range may be higher as the SBC propagated to the edge of model domain on land. These values are very similar to that reported by the Seroka et al. [14] for the New Jersey coast where the initial SBC was ~30 km wide and symmetrically expanded both onshore and offshore to a total width of ~250 km after 7 h. In our study there was a significant asymmetry in the expansion of the SBC. The SBC propagated at maximum speed of 30 kmh^{-1} to 140 km offshore. In contrast, the onshore propagation speed was 10 kmh^{-1} and extended only 30 km inland (Figures 8–10). The maximum expansion speeds of the SBC was reached around 1100 for both onshore and offshore propagation (Figure 11). SBC's have been confirmed to have a preferred location according to the flow regime and local conditions and this study confirmed this through the numerical simulations with the initiation of the SBC at the coast at 115.5° E; 33° S in a region of low winds (Figures 8a and 9a) that may be a result of the local land topography.

In a classical sea breeze system, wind ellipses are expected to be roughly perpendicular to the coastline. Due to the interaction with the synoptic or gradient winds the wind ellipses in the study area were mainly oriented south-west to north-east in the offshore region with slight changes in orientation close to the coast (Figure 16a). In contrast, the presence of land provides a barrier to the ocean currents that flow mainly shore parallel that are reflected in the current ellipses (Figure 16b).

In the study region coastal waves and currents responded to the onset of the sea breeze almost instantaneously [10,12]. The surface currents responded with an increase in velocity and change in direction whilst the depth of current response and lag time after sea breeze onset was dependent on the maximum sea breeze wind speed and duration for which it was sustained above background wind speeds [12]. On the continental shelf, surface currents responded to the LSB forcing but were modified

through topography. In particular, the presence of the Perth canyon and Rottnest Island had a storing influence on the current patterns (Figure 15). In deeper water, the surface currents responded with anticlockwise rotation reflecting similar rotation in wind speed and direction [50]. These findings were confirmed in the results of this study which indicated enhanced anticlockwise spectral energy in both the wind and current fields with the latter more prominent in deeper water (Figure 17). Diurnal surface current ellipses calculated using high frequency radar (HFR) data indicated that over the range of the HFR system (~120 km) there was strong diurnal energy in the surface currents (Figure 13) and thus the offshore extent of the SBC would extend further offshore as confirmed by the WRF model. In the New Jersey coastal ocean, the diurnal wind forced motions extended as far as 100 km offshore [88].

Surface currents generated by wind stress, in combination with the Coriolis force, have a maximum response at the local inertial frequency [89,90]. When the period of wind forcing is close to the local inertial period, a resonance condition occurs. At the latitude 30° (north and south), defined as the 'critical latitude', the inertial period is close to 24 h which often is the period of the LSB. Thus regions close to the 'critical latitude' are regions where diurnal resonance is most likely to occur [85,90–92] (Figure 17). In the study region, the local inertial frequency (22.6 h) is close to the LSB forcing and using field measurements, the presence of near-inertial waves, generated through this diurnal–inertial resonance has been identified [50]. During periods of LSB cycles strong anticlockwise diurnal motions (amplitudes exceeding 0.3 ms^{-1}) were identified and penetrated to water depth ~300 m with diurnal vertical isotherm fluctuations up to 60 m [50].

This study concentrated on the dynamics of the sea breeze cell in the offshore, in particular the offshore extent. Due to the presence of synoptic winds, 'pure' sea breeze events (i.e., onshore winds in the afternoon) were not examined. The logical step for further work to undertake such as study and examine the offshore extent and the ocean response. Similarly, we concentrated on the dynamics at the air-sea interface (surface winds and currents). This could be extended to examine the vertical structure in the atmosphere (i.e., time variability of the vertical structure of the LSB cell) and the vertical structure of the ocean currents (see also [50]).

5. Conclusions

This study examined the spatial-temporal variation of the LSB sea breeze system along the south-west Australian coast that experiences unusually strong and persistent diurnal sea breezes. The emphasis was on the evolution, frontal propagation, and offshore extent of the LSB system and the surface current response. The study was undertaken using field measurements together with atmospheric and ocean numerical models. The main conclusions were as follows:

(a)   The LSB cycle was such that wind speeds decreased between midnight and 0400 and increased rapidly after 1100, reaching maxima >10 ms^{-1} around 1800, decreasing to midnight. Wind directions were such that there were southeasterly winds (120°) in the morning and changing to southerly (~200°) in the afternoon. Although the sea breeze winds (diurnal) were oriented south-west to north-east in combination with the south-easterly gradient winds resulted in the southerly direction.

(b)   The sea breeze cell was initiated within a small area near 115.5° E; 33° S in the morning around 0800 and expanded asymmetrically offshore with maximum speed of 30 kmh^{-1} reaching 120 km offshore. In contrast, the onshore propagation was limited to 30 km at a maximum speed of 10 kmh^{-1}.

(c)   The wind and surface currents rotated anticlockwise with the surface currents responding almost instantaneously to changes in wind forcing but were modified by topography.

Conflicts of Interest: The authors declare no conflict of interest.

References

1. Sonu, C.J.; Murray, S.P.; Hsu, S.A.; Suhayda, J.N.; Waddell, E. Sea breeze and coastal processes. *Eos Trans. Am. Geophys. Union* **1973**, *54*, 820. [CrossRef]
2. Neumann, J. The Coriolis Force in Relation to the Sea and Land Breezes—A Historical Note. *Bull. Am. Meteorol. Soc.* **1984**, *65*, 24–26. [CrossRef]
3. Simpson, J.E. Diurnal Changes in Sea-Breeze Direction. *J. Appl. Meteorol.* **1996**, *35*, 1166–1169. [CrossRef]
4. Davis, W.M.; Schultz, L.C.; Ward, R. An investigation of the sea breeze. *Harv. Univ. Ann. Astron. Obs.* **1890**, *21*, 214–264.
5. Simpson, J.E. *Sea Breeze and Local Winds*; Cambridge University Press: Cambridge, UK, 1994; 234p.
6. Miller, S.T.K.; Keim, B.D.; Talbot, R.W.; Mao, H. Sea breeze: Structure, forecasting, and impacts. *Rev. Geophys.* **2003**, *41*. [CrossRef]
7. Masselink, G.; Pattiaratchi, C.B. Characteristics of the sea breeze system in Perth, Western Australia, and its effect on the nearshore wave climate. *J. Coast. Res.* **2001**, *17*, 173–187.
8. Dampier, W. *Voyages and Descriptions, Vol. II: Capt. Dampier's Discourse of the Trade Winds, Breezes, Storms, Seasons of the Year, Tides and Currents of the Torrid Zone Throughout the World*; Printed for James Knapton: London, UK, 1705; p. 112.
9. Abbs, D.J.; Physick, W.L. Sea breeze observations and modelling: A review. *Aust. Meterological Mag.* **1992**, *41*, 7–19.
10. Pattiaratchi, C.B.; Hegge, B.; Gould, J.; Eliot, I. Impact of sea-breeze activity on nearshore and foreshore processes in southwestern Australia. *Cont. Shelf Res.* **1997**, *17*, 1539–1560. [CrossRef]
11. Masselink, G.; Pattiaratchi, C.B. The effect of sea breeze on beach morphology, surf zone hydrodynamics and sediment resuspension. *Mar. Geol.* **1998**, *146*, 115–135. [CrossRef]
12. Gallop, S.L.; Verspecht, F.; Pattiaratchi, C.B. Sea breezes drive currents on the inner continental shelf off southwest Western Australia. *Ocean Dyn.* **2012**, *62*, 569–583. [CrossRef]
13. Churchill, J.H.; Lentz, S.J.; Farrar, J.T.; Abualnaja, Y. Properties of Red Sea coastal currents. *Cont. Shelf Res.* **2014**, *78*, 51–61. [CrossRef]
14. Seroka, G.; Fredj, E.; Kohut, J.; Dunk, R.; Miles, T.; Glenn, S. Sea Breeze Sensitivity to Coastal Upwelling and Synoptic Flow Using Lagrangian Methods. *J. Geophys. Res. Atmos.* **2018**, *123*, 9443–9461. [CrossRef]
15. Van Der Mheen, M.; Pattiaratchi, C.B.; Cosoli, S.; Wandres, M. Depth-Dependent Correction for Wind-Driven Drift Current in Particle Tracking Applications. *Front. Mar. Sci.* **2020**, *7*, 305. [CrossRef]
16. Woodson, C.B.; Eerkes-Medrano, D.; Flores-Morales, A.; Foley, M.; Henkel, S.; Hessing-Lewis, M.; Jacinto, D.; Needles, L.; Nishizaki, M.; O'Leary, J.; et al. Local diurnal upwelling driven by sea breezes in northern Monterey Bay. *Cont. Shelf Res.* **2007**, *27*, 2289–2302. [CrossRef]
17. Malmaeus, J.M.; Håkanson, L. A dynamic model to predict suspended particulate matter in lakes. *Ecol. Model.* **2003**, *167*, 247–262. [CrossRef]
18. Lawrence, D.; Dagg, M.J.; Liu, H.; Cummings, S.R.; Ortner, P.B.; Kelble, C. Wind events and benthic-pelagic coupling in a shallow subtropical bay in Florida. *Mar. Ecol. Prog. Ser.* **2004**, *266*, 1–13. [CrossRef]
19. Crosman, E.T.; Horel, J.D. Sea and Lake Breezes: A Review of Numerical Studies. *Bound. Layer Meteorol.* **2010**, *137*, 1–29. [CrossRef]
20. Hadi, T.W.; Horinouchi, T.; Tsuda, T.; Hashiguchi, H.; Fukao, S. Sea-Breeze Circulation over Jakarta, Indonesia: A Climatology Based on Boundary Layer Radar Observations. *Mon. Weather. Rev.* **2002**, *130*, 2153–2166. [CrossRef]
21. Hassan, H.; Raman, S. Numerical modelling of coastal circulation near complex topography. *Proc. Indian Natl. Sci. Acad.* **2003**, *69*, 615–632.

22. Shiraki, M. Countetrclockwise rotation of wind hodographs of sea and land breezes in the Kanto plain. *J. Meteorol. Soc. Jpn.* **1986**, *64*, 155–160. [CrossRef]

23. Wilczak, J.M.; Dabberdt, W.F.; Kropfli, R.A. Observations and Numerical Model Simulations of the Atmospheric Boundary Layer in the Santa Barbara Coastal Region. *J. Appl. Meteorol.* **1991**, *30*, 652–673. [CrossRef]

24. Banta, R.M.; Olivier, L.D.; Levinson, D.H. Evolution of the Monterey Bay sea-breeze layer as observed by pulsed Doppler radar. *J. Atmos. Sci.* **1993**, *50*, 3959–3982. [CrossRef]

25. Boybeyi, Z.; Raman, S. A three-dimensional numerical sensitivity study of convection over the Florida peninsula. *Bound. Layer Meteorol.* **1992**, *60*, 325–359. [CrossRef]

26. Wakimoto, R.M.; Atkins, N.T. Observations of the sea Breeze front during CaPE. Part I: Single-doppler, satellite, and cloud photogrammetry analysis. *Mon. Weather Rev.* **1994**, *122*, 1092–1114. [CrossRef]

27. Kalthoff, N.; Bischoff-Gauß, I.; Fiebig-Wittmaack, M.; Fiedler, F.; Thürauf, J.; Novoa, E.; Pizarro, C.; Castillo, R.; Gallardo, L.; Rondanelli, R.; et al. Mesoscale Wind Regimes in Chile at 30°S. *J. Appl. Meteorol.* **2002**, *41*, 953–970. [CrossRef]

28. Pérez, A.; Ortiz, J.C.; Bejarano, L.F.; Otero, L.; Restrepo, J.C.; Franco, A. Sea breeze in the Colombian Caribbean coast. *Atmósfera* **2018**, *31*, 389–406. [CrossRef]

29. Melas, D.; Lavagnini, A.; Sempreviva, A.M. An Investigation of the Boundary Layer Dynamics of Sardinia Island under Sea-Breeze Conditions. *J. Appl. Meteorol.* **2000**, *39*, 516–524. [CrossRef]

30. Cruz, J.; Lorente, J.; Redaño, A. Main features of the sea-breeze in Barcelona. *Meteorol. Atmos. Phys.* **1991**, *46*, 175–179. [CrossRef]

31. Drobinski, P.; Bastin, S.; Dabas, A.; Delville, P.; Reitebuch, O. Variability of three-dimensional sea breeze structure in southern France: Observations and evaluation of empirical scaling laws. *Ann. Geophys.* **2006**, *24*, 1783–1799. [CrossRef]

32. Prtenjak, M.T.; Pasarić, Z.; Orlić, M.; Grisogono, B. Rotation of sea/land breezes along the northeastern Adriatic coast. *Ann. Geophys.* **2008**, *26*, 1711–1724. [CrossRef]

33. Eager, R.E.; Raman, S.; Wootten, A.M.; Westphal, D.L.; Reid, J.S.; Al Mandoos, A. A climatological study of the sea and land breezes in the Arabian Gulf region. *J. Geophys. Res. Space Phys.* **2008**, *113*. [CrossRef]

34. Davis, S.R.; Farrar, J.T.; Weller, R.A.; Jiang, H.; Pratt, L.J. The Land-Sea Breeze of the Red Sea: Observations, Simulations, and Relationships to Regional Moisture Transport. *J. Geophys. Res. Atmos.* **2019**, *124*, 13803–13825. [CrossRef] [PubMed]

35. Steele, C.J.; Dorling, S.R.; von Glasow, R.; Bacon, J. Idealized WRF model sensitivity simulations of sea breeze types and their effects on offshore wind fields. *Atmos Chem. Phys.* **2013**, *13*, 443–461. [CrossRef]

36. Gille, S.T.; Statom, N.M.; Smith, S.G.L. Global observations of the land breeze. *Geophys. Res. Lett.* **2005**, *32*, L05605. [CrossRef]

37. Pielke, R. An overview of our current understanding of the physical interactions between the sea- and land-breeze and the coastal waters. *Ocean Manag.* **1981**, *6*, 87–100. [CrossRef]

38. Bowers, L. *The Effect of Sea Surface Temperature on Sea Breeze Dynamics along the Coast of New Jersey*; Rutgers University: New Brunswick, NJ, USA, 2004.

39. Planchon, O.; Cautenet, S. Rainfall and Sea-Breeze Circulation over South-Western France. *Int. J. Clim.* **1997**, *17*, 535–549. [CrossRef]

40. Tijm, A.B.C.; Holtslag, A.A.M.; Van Delden, A.J. Observations and Modeling of the Sea Breeze with the Return Current. *Mon. Weather Rev.* **1999**, *127*, 625–640. [CrossRef]

41. Findlater, J. Some aerial exploration of coastal airflow. *Meteorol. Mag.* **1963**, *92*, 231–243.

42. Hsu, S.-A. Coastal Airir-Circulation System: Observations and Empirical Model 1,2. *Mon. Weather Rev.* **1970**, *98*, 487–509. [CrossRef]

43. Banta, R. Sea breezes shallow and deep on the Californian coast. *Mon. Weather Rev.* **1995**, *123*, 3614–3622. [CrossRef]

44. Niino, H. The Linear Theory of Land and Sea Breeze Circulation. *J. Meteorol. Soc. Jpn.* **1987**, *65*, 901–921. [CrossRef]

45. Yan, H.; Anthes, R.A. The Effect of Latitude on the Sea Breeze. *Mon. Weather Rev.* **1987**, *115*, 936–956. [CrossRef]

46. Ciesielski, P.E.; Schubert, W.H.; Johnson, R.H. Diurnal Variability of the Marine Boundary Layer during ASTEX. *J. Atmos. Sci.* **2001**, *58*, 2355–2376. [CrossRef]

47. Gille, S.T.; Lee, S.M.; Smith, S.G.L. Measuring the sea breeze from QuikSCAT Scatterometry. *Geophys. Res. Lett.* **2003**, *30*, 1114. [CrossRef]

48. Finkele, K.; Kraus, H.; Byron-Scott, R.A.D. A complete sea-breeze circulation cell derived from aircraft observations. *Bound. Layer Meteorol.* **1995**, *73*, 299–317. [CrossRef]

49. Zaker, N.H.; Imberger, J.; Pattiaratchi, C.B. Dynamics of the Coastal Boundary Layer off Perth, Western Australia. *J. Coast. Res.* **2007**, *23*, 1112–1130. [CrossRef]

50. Mihanović, H.; Pattiaratchi, C.B.; Verspecht, F. Diurnal Sea Breezes Force Near-Inertial Waves along Rottnest Continental Shelf, Southwestern Australia. *J. Phys. Oceanogr.* **2016**, *46*, 3487–3508. [CrossRef]

51. Verspecht, F.; Pattiaratchi, C.B. On the significance of wind event frequency for particulate resuspension and light attenuation in coastal waters. *Cont. Shelf Res.* **2010**, *30*, 1971–1982. [CrossRef]

52. Pattiaratchi, C.B.; Eliot, M.; Smith, J.M. Sea Level Variability in South-West Australia: From Hours to Decades. In *Proceedings of the Coastal Engineering 2008*; World Scientific Pub Co Pte Ltd.: Singapore, 2009; pp. 1186–1198.

53. Cosoli, S.; Pattiaratchi, C.B.; Hetzel, Y. High-Frequency Radar Observations of Surface Circulation Features along the South-Western Australian Coast. *J. Mar. Sci. Eng.* **2020**, *8*, 97. [CrossRef]

54. Pattiaratchi, C.B.; Woo, M. The mean state of the Leeuwin Current system between North West Cape and Cape Leeuwin. *J. Roy. Soc. West. Aust.* **2009**, *92*, 221–241.

55. Ridgway, K.R.; Condie, S.A. The 5500-km-long boundary flow of western and southern Australia. *J. Geophys. Res. Oceans* **2009**, *109*, C04017. [CrossRef]

56. Wijeratne, E.M.S.; Pattiaratchi, C.B.; Proctor, R. Estimates of Surface and Subsurface Boundary Current Transport Around Australia. *J. Geophys. Res. Oceans* **2018**, *123*, 3444–3466. [CrossRef]

57. Pearce, A.; Pattiaratchi, C.B. The Capes Current: A summer countercurrent flowing past Cape Leeuwin and Cape Naturaliste, Western Australia. *Cont. Shelf Res.* **1999**, *19*, 401–420. [CrossRef]

58. Tapper, N.; Hurry, L. *Australia's Weather Patterns: An Introductory Guide*; Dellasta Pty Ltd.: Melbourne, Australia, 1993; p. 130.

59. Kepert, J.D.; Smith, R.K. A Simple Model of the Australian West Coast Trough. *Mon. Weather Rev.* **1992**, *120*, 2042–2055. [CrossRef]

60. Edwards, C.R. Coastal Ocean Response to Near-Resonant Sea Breeze/Land Breeze Near the Critical Latitude in the Georgia Bight. Ph.D. Thesis, University of North Carolina-Chapel Hill, Chapel Hill, NC, USA, 2008.

61. Lerczak, J.A.; Hendershott, M.C.; Winant, C.D. Observations and modeling of coastal internal waves driven by a diurnal sea breeze. *J. Geophys. Res. Space Phys.* **2001**, *106*, 19715–19729. [CrossRef]

62. Crombie, D.D. Doppler Spectrum of Sea Echo at 13.56 Mc./s. *Nat. Cell Biol.* **1955**, *175*, 681–682. [CrossRef]

63. Barrick, D.E.; Evans, M.W.; Weber, B.L. Ocean Surface Currents Mapped by Radar. *Science* **1977**, *198*, 138–144. [CrossRef]

64. Hammond, T.; Pattiaratchi, C.B.; Eccles, D.; Osborne, M.; Nash, L.; Collins, M. Ocean surface current radar (OSCR) vector measurements on the inner continental shelf. *Cont. Shelf Res.* **1987**, *7*, 411–431. [CrossRef]

65. Paduan, J.D.; Washburn, L. High-Frequency Radar Observations of Ocean Surface Currents. *Annu. Rev. Mar. Sci.* **2013**, *5*, 115–136. [CrossRef]

66. Cosoli, S.; Grcic, B.; De Vos, S.; Hetzel, Y. Improving Data Quality for the Australian High Frequency Ocean Radar Network through Real-Time and Delayed-Mode Quality-Control Procedures. *Remote Sens.* **2018**, *10*, 1476. [CrossRef]

67. Mahjabin, T.; Pattiaratchi, C.B.; Hetzel, Y.; Janeković, I. Spatial and Temporal Variability of Dense Shelf Water Cascades along the Rottnest Continental Shelf in Southwest Australia. *J. Mar. Sci. Eng.* **2019**, *7*, 30. [CrossRef]

68. Skamarock, W.C.; Klemp, J.B.; Dudhia, J.; Gill, D.O.; Barker, D.M.; Duda, M.G.; Huang, X.Y.; Wang, W.; Powers, J.G. *A Description of the Advanced Research WRF Version 3*; NCAR Technical Note, NCAR/TN-475+STR; Mesoscale and Microscale Meteorology Division, National Center for Atmospheric Research: Boulder, CO, USA, 2008.

69. Challa, V.S.; Indracanti, J.; Rabarison, M.K.; Patrick, C.; Baham, J.M.; Young, J.; Hughes, R.; Hardy, M.G.; Swanier, S.J.; Yerramilli, A. A simulation study of mesoscale coastal circulations in Mississippi Gulf coast. *Atmos. Res.* **2009**, *91*, 9–25. [CrossRef]

70. Wicker, L.J.; Skamarock, W.C. Time-Splitting Methods for Elastic Models Using Forward Time Schemes. *Mon. Weather Rev.* **2002**, *130*, 2088–2097. [CrossRef]

71. Janekovic, I. An atmospheric and oceanic forecast system for the west coast of Australia. (in prep)

72. Shchepetkin, A.F.; McWilliams, J.C. The regional oceanic modeling system (ROMS): A split-explicit, free-surface, topography-following-coordinate oceanic model. *Ocean Model.* **2005**, *9*, 347–404. [CrossRef]

73. Shchepetkin, A.F.; McWilliams, J.C. Correction and commentary for "Ocean forecasting in terrain-following coordinates: Formulation and skill assessment of the regional ocean modeling system" by Haidvogel et al., J. Comp. Phys. 227, pp. 3595–3624. *J. Comput. Phys.* **2009**, *228*, 8985–9000. [CrossRef]

74. Whiteway, T.G. Australian Bathymetry and Topography Grid. *Geosci. Aust. Rec.* **2009**, *2009*, 46.

75. Sikirić, M.D.; Janeković, I.; Kuzmić, M. A new approach to bathymetry smoothing in sigma-coordinate ocean models. *Ocean Model.* **2009**, *29*, 128–136. [CrossRef]

76. Egbert, G.D.; Erofeeva, S.Y. Efficient Inverse Modeling of Barotropic Ocean Tides. *J. Atmos. Ocean. Technol.* **2002**, *19*, 183–204. [CrossRef]

77. Flather, R.A. A tidal model of the north-west European continental shelf. *Mem. Soc. R. Sci. Liege* **1976**, *6*, 141–164.

78. Marchesiello, P.; McWilliams, J.C.; Shchepetkin, A.F. Open boundary conditions for long-term integration of regional oceanic models. *Ocean Model.* **2001**, *3*, 1–20. [CrossRef]

79. Smolarkiewicz, P.K.; Margolin, L.G. MPDATA: A Finite-Difference Solver for Geophysical Flows. *J. Comput. Phys.* **1998**, *140*, 459–480. [CrossRef]

80. Fairall, C.W.; Bradley, E.F.; Rogers, D.P.; Edson, J.B.; Young, G.S. Bulk parameterization of air-sea fluxes for Tropical Ocean-Global Atmosphere Coupled-Ocean Atmosphere Response Experiment. *J. Geophys. Res. Space Phys.* **1996**, *101*, 3747–3764. [CrossRef]

81. Pattiaratchi, C.B.; Wijeratne, E.M.S. Tide gauge observations of the 2004–2007 Indian Ocean tsunamis from Sri Lanka and Western Australia. *Pure Appl. Geophys.* **2009**, *166*, 233–258. [CrossRef]

82. Emery, W.J.; Thomson, R.E. *Data Analysis Methods in Physical Oceanography*; Elsevier: Amsterdam, The Netherlands, 1994.

83. Nam, S.; Send, U. Resonant Diurnal Oscillations and Mean Alongshore Flows Driven by Sea/Land Breeze Forcing in the Coastal Southern California Bight. *J. Phys. Oceanogr.* **2013**, *43*, 616–630. [CrossRef]

84. Gonella, J. A rotary-component method for analysing meteorological and oceanographic vector time series. *Deep. Sea Res. Oceanogr. Abstr.* **1972**, *19*, 833–846. [CrossRef]

85. Hyder, P.; Simpson, J.H.; Xing, J.; Gille, S.T. Observations over an annual cycle and simulations of wind-forced oscillations near the critical latitude for diurnal–inertial resonance. *Cont. Shelf Res.* **2011**, *31*, 1576–1591. [CrossRef]

86. Calmet, I.; Mestayer, P.G.; Van Eijk, A.M.J.; Herlédant, O. A Coastal Bay Summer Breeze Study, Part 2: High-resolution Numerical Simulation of Sea-breeze Local Influences. *Bound. Layer Meteorol.* **2017**, *167*, 27–51. [CrossRef]

87. Atkinson, B.W. *Meso-Scale Atmospheric Circulations*; Academic Press: London, UK, 1981; p. 495.

88. Hunter, E.; Chant, R.; Bowers, L.; Glenn, S.; Kohut, J. Spatial and temporal variability of diurnal wind forcing in the coastal ocean. *Geophys. Res. Lett.* **2007**, *34*. [CrossRef]

89. Ekman, V.W. On the influence of the earth's rotation on ocean currents. *Ark. Mat. Astron. Fys.* **1905**, *2*, 1–52.

90. Simpson, J.H.; Hyder, P.; Rippeth, T.P.; Lucas, I.M. Forced Oscillations near the Critical Latitude for Diurnal-Inertial Resonance. *J. Phys. Oceanogr.* **2002**, *32*, 177–187. [CrossRef]

91. Zhang, X.; Di Marco, S.F.; Smith, D.C.; Howard, M.K.; Jochens, A.E.; Hetland, R.D. Near-Resonant Ocean Response to Sea Breeze on a Stratified Continental Shelf. *J. Phys. Oceanogr.* **2009**, *39*, 2137–2155. [CrossRef]

92. Kim, S.Y.; Crawford, G. Resonant ocean current responses driven by coastal winds near the critical latitude. *Geophys. Res. Lett.* **2014**, *41*, 5581–5587. [CrossRef]